2011

Small-Signal Modeling of Resonant Converters

Agasthya Ayachit
Wright State University

SMALL-SIGNAL MODELING OF RESONANT CONVERTERS

A thesis submitted in partial fulfillment

of the requirements for the degree of

Master of Science in Engineering

By

Agasthya Ayachit

B. E., Visvesvaraya Technological University, Belgaum, India, 2009

2011

Wright State University

WRIGHT STATE UNIVERSITY
SCHOOL OF GRADUATE STUDIES

July 15, 2011

I HEREBY RECOMMEND THAT THE THESIS PREPARED UNDER MY SUPERVISION BY Agasthya Ayachit ENTITLED Small-signal Modeling of Resonant Converters BE ACCEPTED IN PARTIAL FULFILLMENT OF THE REQUIREMENTS FOR THE DEGREE OF Master of Science in Engineering.

Marian K. Kazimierczuk, Ph.D.

Thesis Director

Kefu Xue, Ph.D.

Chair
Department of Electrical Engineering
College of Engineering and Computer Science

Committee on
Final Examination

Marian K. Kazimierczuk, Ph.D.

Kuldip Rattan, Ph.D.

Saiyu Ren, Ph.D.

Andrew Hsu, Ph.D.
Dean, School of Graduate Studies

Abstract

Ayachit, Agasthya. M.S.Egr, Department of Electrical Engineering, Wright State University, 2011. *Small-Signal Modeling of Resonant Converters.*

Resonant DC-DC converters play an important role in applications that operate at high-frequencies (HF). Their advantages over those of pulse-width modulated (PWM) DC-DC converters have led to the invention of several topologies over the traditional forms of these converters. Series resonant converter is the subject of study in this thesis. By variation in the switching frequency of the transistor switches, the optimum operating points can be achieved. Hence, the steady-state frequency-domain analysis of the series resonant converter is performed. The operational and characteristic differences between the series resonant and parallel resonant and series-parallel resonant configurations are highlighted. In order to understand the converter response for fluctuations in their input or control parameters, modeling of these converters becomes essential. Many modeling techniques perform analysis only in frequency-domain. In this thesis, the extended describing function method is used, which implements both frequency-domain and time-domain analysis. Based on the first harmonic approximation, the steady-state variables are derived. Perturbing the steady-state model about their operating point, a large-signal model is developed. Linearization is performed on the large-signal model extracting the small-signal converter state variables. The small-signal converter state variables are expressed in the form of the transfer matrix. Finally, a design example is provided in order to evaluate the steady-state parameters. The converter is simulated using SABER Sketch circuit simulation software and the steady-state parameters are plotted to validate the steady-state parameters. It is observed that the theoretical steady-state values agrees with the simulated results obtained using SABER Sketch.

Contents

List of Figures

Acknowledgement

First and foremost, I would like to express my sincerest gratitude to my advisor Dr. Marian K. Kazimierczuk, whose support, patience, and kindness has helped me benefit the most out of this thesis. My heartfelt thank you to him.

I wish to thank my committee members, Dr. Kuldip Rattan and Dr. Saiyu Ren, for giving me valuable suggestions and advice on this thesis.

My sincere regards to my parents whose support and encouragement have been invaluable.

The present research met its pace with constant guidance and motivation by my fellow colleagues, Dr. Dakshina Murthy Bellur and Veda Prakash Galigekere. My heartfelt thanks and best wishes to them. I would also like to thank Dhivya A. N and Rafal Wojda who have helped me with the documentation and other technical concerns.

Last but not the least, my thanks to all my friends who have helped me be at the right place and at the right time.

1 Introduction

1.1 Resonant Converters

Resonant converters are being used extensively in high-frequency DC-DC and dc-ac converters due to several advantages such as zero-voltage and zero-current switching, fast dynamic response, and reduced electro-magnetic interference [1]. These converters find their use in several high-frequency applications in aerospace, military, communication systems and so on. In the present day industry, resonant converters are widely used in the light emitting diode (LED) driver circuits. They should provide constant current since the brightness of LEDs are current-dependent. Some resonant converter topologies provide DC isolation and this becomes essential when the load needs to be completely isolated from the input and power stages of the converter. These converters are usually operated between tens of kilohertz to several mega hertz. Due to this high frequency switching, size of the components is reduced by a large extent thus improving the power density. The effect of parasitic capacitances of switches and parasitic inductances of the transformers used in resonant converters will be reduced since they become a part of the resonant components. The most important advantage of the resonant converters being their switching losses when compared with that of pulse-width modulated (PWM) converters. Resonant converters are designed to efficiently operate at zero-voltage and zero-current modes of switching, which reduces the switching losses by a very significant factor and thereby improving the efficiency. These soft switching techniques reduces the voltage and current stresses of the switches and diodes improving their operational capabilities and life-spans. Resonant converters can be classified based on their circuit characteristics and operation as

- Quasi-resonant converters (QRC)

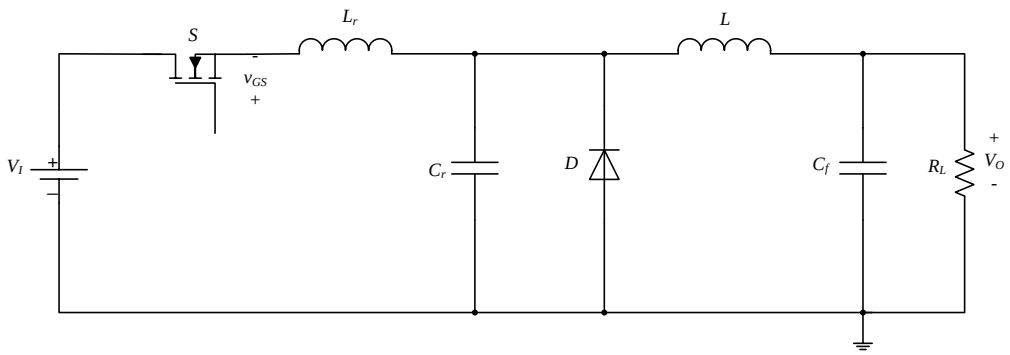

Figure 1.1: Quasi-resonant buck converter.

- Traditional resonant converters

Although the PWM DC-DC converters give out high amount of losses at higher switching frequencies, the switches in them can be modified using resonant components such that they operate as resonant switches and possess properties which favour in improving the efficiency. These converters are known as quasi-resonant converters. A basic circuit diagram of a quasi-resonant buck converter is shown in Figure 1.1. By introducing a resonant network in series or parallel to the controlled switch in PWM converter, a zero-current switching or a zero-voltage switching QRC, respectively, can be obtained. With the use of these resonant switches, higher operating frequencies can be achieved. More detailed explanation about quasi-resonant switches and quasi-resonant DC-DC converters is provided in [2].

The traditional converters include series resonant (SRC), parallel resonant (PRC) and series-parallel resonant (SPRC) converters. The basic block diagram of a typical resonant converter is shown in Figure 1.2. These converters consist of a network of inductors and capacitors connected in different patterns between the switching network (inverter stage) and the output network (rectifier stage). These passive components act as energy storage elements which process the energy and transfer it to the load during different intervals of the switching period. The inverting stage is a half-bridge or a full-bridge network of switches formed usually using MOSFETs or IGBTs. They are unidirectional or bi-directional semiconductor switches. If MOSFETs are used, their body diodes act as anti-parallel diodes. The resonant network is series, parallel or series-parallel connection of inductors and capacitors. The rectifier could be a half-wave or a full-wave network of diodes which are usually connected through a transformer. The later part of the rectifier is equipped with a filter network in order to reduce the ripple content at the output and limit the output current.

1.2 Need for Small-signal Modeling of Converters

DC-DC converters are subjected to certain demands namely, load regulation, line regulation, stability, and response-time taken to achieve steady-state after introducing disturbance into the system either by the input stage or the control stage. Most of these converters can be analysed using either familiar linear circuit theory techniques or other analytical methods of modeling. The small-signal model will provide complete details about the circuit during different intervals of time which will be helpful in understanding its behaviour for variations in the circuit parameters [3]. Both PWM and resonant DC-DC converters consists of components, for example, switches and diodes, which are highly non-linear. In order to apply the linear circuit theory, it is essential to linearize and average those components. The two main modeling techniques that are applicable to both classes of converters are

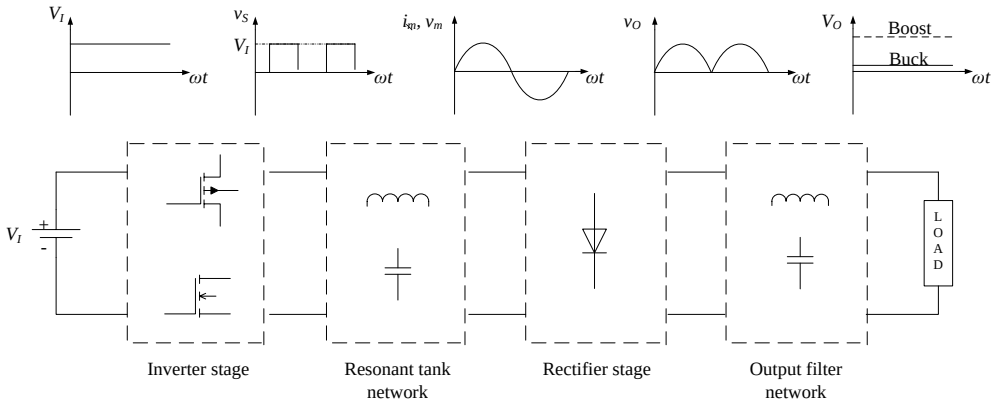

Figure 1.2: Basic block diagram of the traditional resonant converters.

- State-space averaging technique
- Circuit averaging technique

Complete analysis in the DC domain of the series resonant converter has been provided in [6], [7]. Detailed explanation about these techniques are provided in [8] - [11]. Several methods are developed for modeling resonant converters. A complete small-signal analysis of the series and parallel resonant converters have been discussed extensively in [4], [5]. Sampled data modeling techniques were introduced in [12], [13]. Discrete modeling techniques were introduced in [14]. All these modeling techniques involved time-domain analysis and requires mathematical computation and computer software for their implementation. Also, the modeling methods are applicable upto half the switching frequencies only. In order to improve the accuracy and obtain a

model both in frequency-domain and time-domain, the extended describing function method was introduced. This modeling technique helps us realize both frequency control and duty-cycle control [23]. In this thesis, extended describing function method is used for deriving the small-signal model of the resonant converters. Description about this modeling technique is provided in detail in Chapter 4.

1.3 Motivation for Thesis

Modeling of frequency controlled converters has always been a challenge for power electronics researchers. Resonant converters are characterized by one slow moving pole due to the output filter C_f and fast moving poles due to the energy storing resonant elements (L and C). This results in difference in frequencies between the two stages of the circuit. The difference in frequencies between the resonant network and the filter network introduces certain factor of complexity which relegates the usage of several modeling techniques. Hence, with course of time and literature survey, a widely used modeling technique, extended describing function (EDF) was studied. The applicability of this method both in time-domain and frequency-domain is an advantage over other modeling methods. The series resonant converters are used in wide variety of applications. Therefore, the EDF modeling technique is implemented on the series resonant converters in order to obtain the small-signal model and understand their behaviour due to small-signal variations.

1.4 Thesis Objectives

In Chapter 2, the series resonant converter is introduced along with its operation and characteristics. Frequency-domain analysis of the SRC is also provided in Chapter 2. Chapter 3 describes about parallel resonant and series-parallel resonant converters. Their current, voltage and current stresses, and efficiency are discussed and applications mentioned. Chapter 4 emphasizes on the small-signal modeling of fre-

quency controlled converters. The technique behind modeling resonant converters using extended describing function method is discussed. Furthermore, this method is implemented on series resonant converters. Chapter 5, provides a design example of the series resonant converter. The steady-state parameters are determined and verified using SABER Sketch circuit simulator. The steady-state parameters that are derived using extended describing function method are calculated. Finally, Chapter 6 provides the conclusion of the present work and suggests future work.

2 Series Resonant DC-DC Converter

2.1 Introduction to Series Resonant Converter

The classical series resonant converter (SRC) is a frequency controlled converter. It has been widely used in several applications for regulating and converting DC energy provided at its input into DC energy of different levels at its output. Power transfer from source to load is accomplished by rectification of current flowing through the resonant $L-C$ elements using a rectifier network. The operation of SRC is similar to a buck converter where the output voltage is less than the input voltage except at one particular operating point. Different output voltages can be obtained by variation of the switching frequency. The SRC can be modeled as a cascade connection of switching inverter stage, resonant network, and the rectifier stage. The inverter switching stage is either a half-bridge or full-bridge network of switches that is ON for 50 % duty-cycle. The series resonant $L-C$ network acts as a band-pass filter accommodating only those frequencies which are near the resonant frequency. The quality factor determines the selectivity of these frequencies. The rectifier network can either be a half-wave or a full-wave network of diodes connected in order to obtain a unidirectional signal at the output. These are current-driven rectifiers, the operation of which is dependant on the current through the resonant circuit. Depending upon the application, appropriate configuration is considered.

SRC are used widely in several applications ranging from radio-sets to space-crafts. They are used in radio transmitters, electronic ballasts used in fluorescent lamps, induction welding, surface hardening, soldering, annealing, induction seals for tamper-proof packaging, fibre-optics production, dielectric heating for plastic welding, and so on. Presently, they are also being used to supply and regulate power to data storing servers owing to their advantages over other forms of DC-DC converters.

2.1.1 Characteristics of Series Resonant Converter

The series resonant converter is characterized by their resonant frequency f_o, characteristic impedance Z_o, and quality factor Q_L and are expressed as,

$$f_o = \frac{1}{2\pi\sqrt{LC}},$$
$$Z_o = \sqrt{\frac{L}{C}},$$
$$Q_L = \frac{Z_o}{R},$$

where L and C are the inductance (in henry) and capacitance (in farad) of the series resonant circuit respectively, and R is the effective resistance offered to the converter (in ohms). The switching frequency f determines whether the converter operates above, below, or at resonant frequency f_o. The quality factor determines the selectivity of frequencies by this converter. Higher the value of Q_L, more selective the system is towards particular frequencies reducing the band-width.

As the frequency f is less than f_o, the capacitive reactance is dominant and the impedance offered to the current will be capacitive in nature. As a result, the current leads the voltage by certain phase ψ. On the other hand, when the switching frequency f is above f_o, then the impedance offered will be more inductive in nature causing the current to lag the applied voltage by an angle ψ. However, when switching frequency f equals f_o, both the inductive and capacitive reactances will be in quadrature and their voltages V_L and V_C are equal and opposite. At this point, the circuit offers zero reactance to the current and the total impedance will be equal to only the parasitic resistances of the circuit components.

2.2 Circuit Description

The circuit of the SRC is as shown in Figure 2.1. The converter consists of a half-bridge network of bi-directional switches S_1 and S_2. These switches are capable of

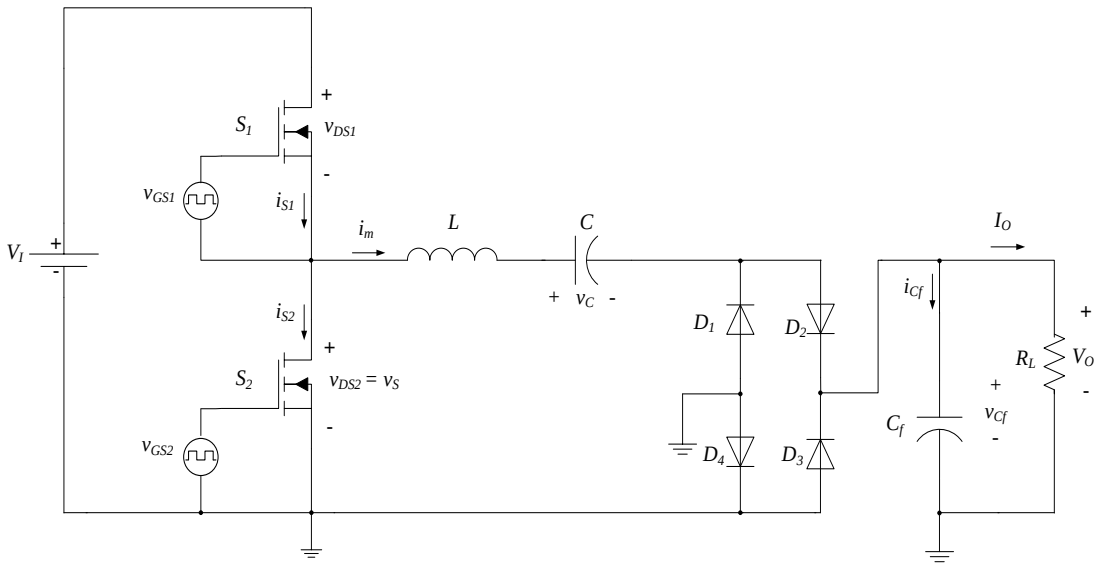

Figure 2.1: Circuit diagram of series resonant converter.

conducting current in both directions. Usually, MOSFETs are used as bi-directional switches. They consist of intrinsic body diodes that can conduct current in the opposite direction to ease flow towards the source. In case other switches like IGBT, BJT are used, then an anti-parallel diode needs to be connected across them for the reverse current to flow towards the source. These diodes should be capable of withstanding the reverse-recovery spikes that are generated during transistor turn-off. The circuit is powered by a DC voltage source V_I. Depending on the application, the DC input could either be a rectified signal from the ac line supply or if they are used in off-line applications, they can be supplied using batteries or fuel cells or connected

as a load to other power converters. The switches are turned on and off using non-overlapping pulses v_{GS1} and v_{GS2} operating under a duty-cycle of 0.5 and at a time period given by $T = 1/f$. The periodic turn-on and turn-off of these switches results in a square-wave voltage $v_s = v_{DS2}$ to appear across S_2. This voltage is supplied as input to the series resonant circuit consisting of inductance L and capacitance C as shown in Figure 2.1. The bridge rectifier network is activated by the alternating high and low voltages appearing across the resonant circuit output. A DC-DC transformer is connected before the bridge rectifier. The rectified voltage is delivered to the load resistance R_L. A capacitor filter C_f is connected at the output in order to eliminate the ripple and block the ac component from flowing to the output. The circuit of SRC depicting the equivalent series resistance (esr) and stages of operation is provided in Figures 2.2 and 2.3. The MOSFETs can be modeled as an ideal switch in series with on-state resistances r_{DS1} and r_{DS2}. r_C and r_L are the esr of the resonant L and C. The esr of C_f is represented as r_{Cf}. A forward-biased diode can be modeled as a forward voltage drop V_F in series with forward resistance R_F.

2.2.1 Assumptions for Analysis

- The loaded quality factor Q_L of the inductance is considered to be high in order to obtain sinusoidally varying i_m.

- The transistor and diode are considered to be resistive in nature and their parasitic capacitance effects as well as switching times are considered to be equal to zero.

- The resonant components L and C are passive, linear and time-invariant. They do not possess any parasitic reactive components.

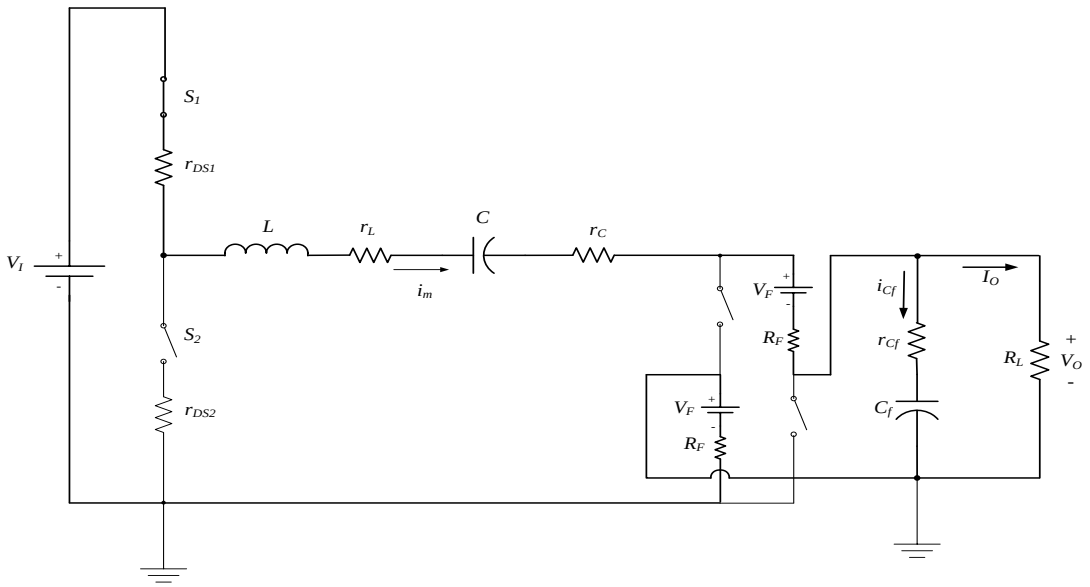

Figure 2.2: Circuit diagram of series resonant converter when S_1 is ON and S_2 is OFF.

2.2.2 Operation

Figure 2.4 depicts the waveforms of currents and voltages for the entire switching period from 0 to 2π. The DC voltage source V_I energizes the converter. Referring to Figure 2.2, when the switch S_1 is turned on during the interval $0 \leq \omega t \leq \pi$, the current flows through the switch and the resonant circuit. Since the source terminal of S_2 is connected to the ground, a maximum voltage of V_I appears across it driving the resonant current. Because of the high quality factor of the inductor, the current i_m is sinusoidal. This sinusoidally varying current i_m at the rectifier terminals forces the two diodes from different legs to turn-on periodically. When $i_m > 0$, then D_2, D_4 are forward-biased and D_1, D_3 are reverse-biased. The flow of current is represented by solid lines. The voltage appearing across the rectifier output is unidirectional pulsating output voltage with an average value V_O. The filter capacitor C_f eliminates

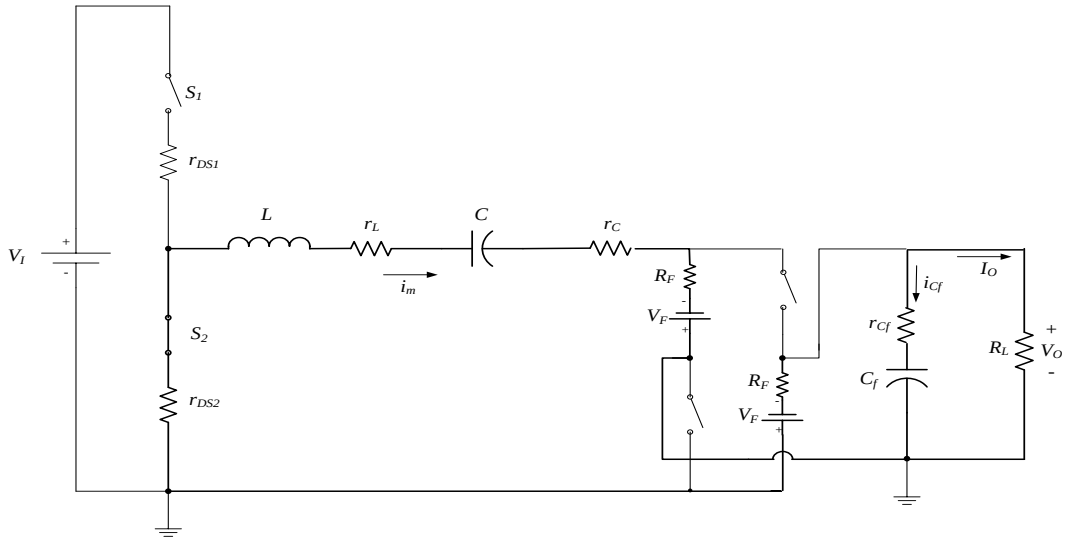

Figure 2.3: Circuit diagram of series resonant converter when S_1 is OFF and S_2 is ON.

the ac component from this signal providing a constant DC at the output.

During the time interval $\pi \leq \omega t \leq 2\pi$, the switch S_1 is OFF and S_2 is turned on. The voltage $v_s = v_{DS2}$ is now equal to 0. The current circulates through the resonant circuit and the switch S_2 as shown in Figure 2.3. The energy stored in the resonant elements is now discharged through the output path. During this instant, $i_m < 0$, causing D_2, D_4 to be reverse-biased and D_1, D_3 to be forward-biased. The current path is depicted by solid lines.

2.2.3 Modes of Operation

The SRC can be operated in two ranges of frequencies apart from at resonant frequency. Depending upon the demand, the switching frequency f varies with respect to f_o. It can either be below or above f_o. At f_o, the MOSFETs turn-on and turn-off

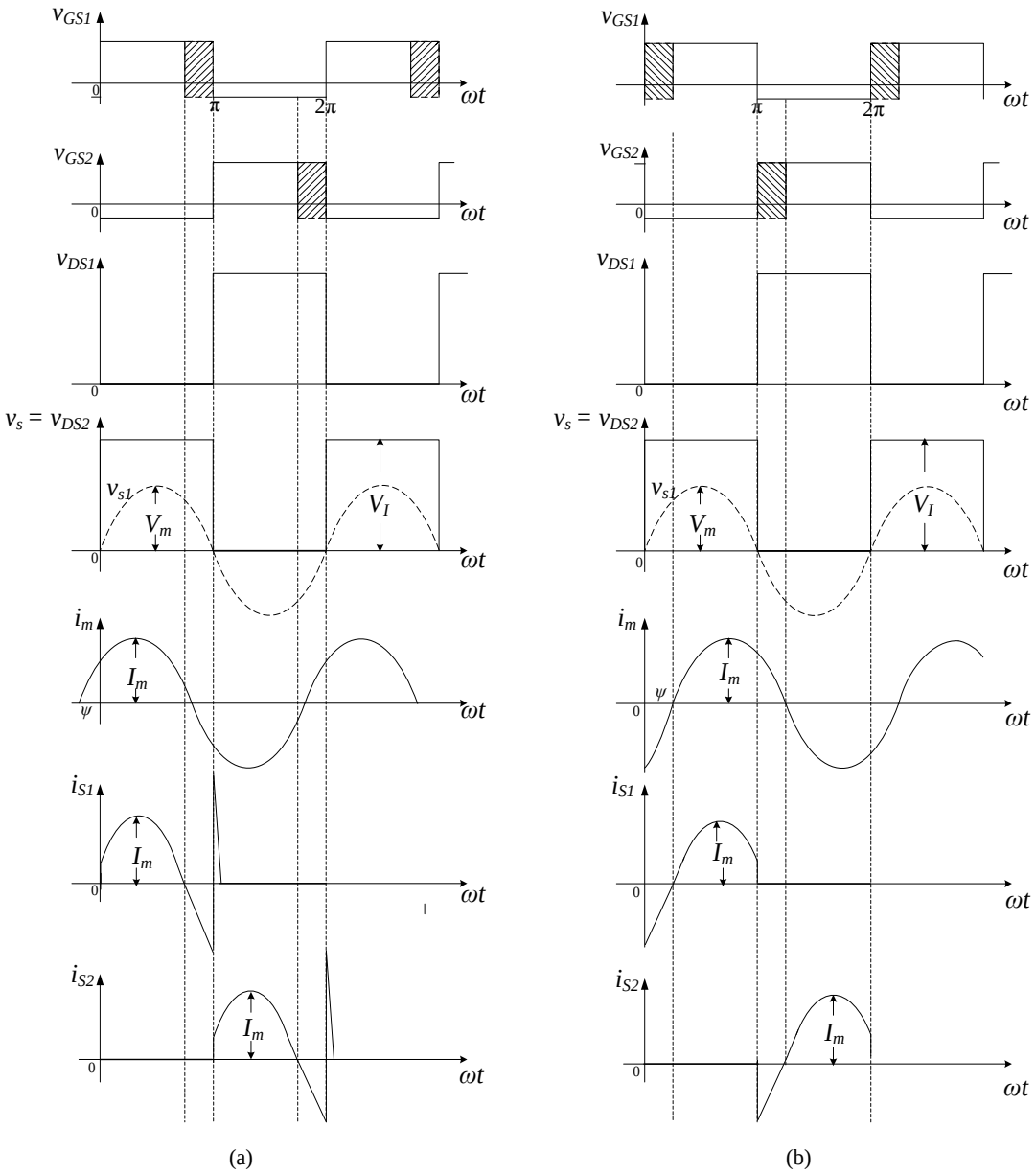

Figure 2.4: Current and voltage waveforms at frequencies (a) below f_o (b) above f_o

exactly at zero-current reducing the stresses across the switches and improving the efficiency. The reverse currrent does not exist in this situation. Detailed explanation about these modes of operation is provided in [15]. The current and voltage waveforms are depicted in Figure 2.4.

- Operation below resonance

  For all frequencies $f < f_o$, the series resonant circuit presents a capacitive load. Hence, the current i_m flowing though the resonant circuit would lead the fundamental component of v_s by certain phase ψ, where $\psi < 0$. The MOSFETs consist of intrinsic body-drain diode for the reverse current to flow through it. However, at frequencies below resonant frequencies, the turn-off of diode causes large dv/dt and di/dt stresses resulting in reverse-recovery spikes as shown in Figure 2.4. Since the resonant inductor L does not allow sudden changes in current, the reverse-recovery current flows through the switch that turns on next. These spikes are about 10 times that of normal value causing stresses across the switches and damaging them.

  Another drawback of operating the converter at $f < f_o$ is the presence of output capacitance C_O across the MOSFET. Before transistor turns on, C_O is charged to a value equal to V_I. After the transistor is turned on, this capacitance finds a path to discharge through the transistor on-state resistance causing turn-on switching losses. Per transistor, the turn-on switching loss is expressed as

  $$P_{turn-on} = 0.5 f C_O V_I^2,$$

  where f is the switching frequency and V_I is the input voltage. A major advantage of below resonant frequency operation is the zero turn-off switching losses. Here, the MOSFETs are turned off at nearly zero voltage resulting in zero-voltage switching (ZVS). The drain current is noticeably low and the drain to source voltage is almost zero during turn-off resulting in ZVS condition.

- Operation above resonance

  As f is above f_o, the resonant circuit offers an inductive load to the flow of current i_m. Under such situations, the fundamental component of voltage v_s leads the current by certain phase ψ, where $\psi > 0$. The turn-on switching loss is almost equal to zero in this range of frequencies. The Miller effect is also absent because of which the input capacitance does not increase requiring less gate-drive power and resulting in reduced turn-on times [1]. Unlike in the case of below resonant frequency operation, the transistor turns off at low di/dt. Hence reverse-recovery spike flowing through the devices is nearly zero, which reduces the necessity for heavy-current devices.

2.3 Steady-state Voltage and Currents of Series Resonant Converter

This section describes the voltages and currents related to the different components of the SRC. The square-wave voltage appearing across the input to the resonant circuit can be expressed as

$$v_{DS2} = v_s = \begin{cases} V_I, & \text{for} \quad 0 < \omega t \leq \pi \\ 0, & \text{for} \quad \pi < \omega t \leq 2\pi \end{cases} \tag{2.1}$$

This voltage v_S appears across switch S_2 as shown in Figure 2.4. The fundamental component of v_S varies sinusoidally with time and for the half-bridge inverter it is given by

$$v_{s1} = V_s \sin\omega t, \tag{2.2}$$

where V_s is the amplitude of the fundamental component v_{s1} and given by

$$V_s = \frac{2V_I}{\pi}.$$

The periodic turn-on and turn-off of S_1 and S_2 results in the flow of current i_m through the resonant circuit. The current is sinusoidal because of high Q_L of resonant

inductance L. Depending on the mode of operation, i_m is either in phase with v_{s1} or out of phase by certain phase ψ and is expressed as

$$i_m = I_m \sin(\omega t - \psi), \tag{2.3}$$

where I_m is the amplitude of the current i_m.

As shown in Figure 2.4, the switch currents i_{S1} and i_{S2} are given by

$$\begin{aligned} i_{S1} = i_m = I_m \sin(\omega t - \psi), \qquad & \text{for} \quad 0 < \omega t \leq \pi, \\ i_{S2} = i_m = I_m \sin(\omega t - \psi), \qquad & \text{for} \quad \pi < \omega t \leq 2\pi. \end{aligned} \tag{2.4}$$

As a result, for the period $0 \rightarrow 2\pi$

$$i_m = i_{S1} - i_{S2}. \tag{2.5}$$

Voltage across inductor L is

$$\begin{aligned} i_L = i_m &= \frac{1}{L} \int_0^{2\pi} v_L(t) dt, \\ v_L &= L \frac{di}{dt}. \end{aligned} \tag{2.6}$$

Voltage across capacitor C is

$$\begin{aligned} i_C = i_m &= C \frac{dv_c}{dt}, \\ v_c &= \frac{1}{C} \int_0^{2\pi} i_m(t) dt. \end{aligned} \tag{2.7}$$

The waveform of voltages across the diodes in the bride rectifier is shown in Figure 2.5. It can be observed that the maximum value of reverse voltages appearing across the diodes is equal to the output voltage V_o given by

$$\begin{aligned} v_{D_2} = v_{D_4} &= \begin{cases} -V_o & \text{for} \quad 0 < \omega t \leq \pi \\ 0 & \text{for} \quad \pi < \omega t \leq 2\pi, \end{cases} \\ v_{D_1} = v_{D_3} &= \begin{cases} 0 & \text{for} \quad 0 < \omega t \leq \pi \\ -V_o & \text{for} \quad \pi < \omega t \leq 2\pi. \end{cases} \end{aligned} \tag{2.8}$$

The current through the diodes is

$$i_{D_1} = i_{D_3} = \begin{cases} I_m \sin(\omega t - \psi), & \text{for} \quad 0 < \omega t \leq \pi \\ 0 & \text{for} \quad \pi < \omega t \leq 2\pi, \end{cases}$$

$$i_{D_2} = i_{D_4} = \begin{cases} 0, & \text{for} \quad 0 < \omega t \leq \pi \\ I_m \sin(\omega t - \psi) & \text{for} \quad \pi < \omega t \leq 2\pi. \end{cases} \tag{2.9}$$

The DC component of the output current is derived by considering the average value of the rectifier output current in one switching cycle given as

$$I_O = \frac{1}{2\pi} \int_0^{2\pi} i_{D1} d(\omega t) = \frac{I_m}{2\pi} \int_0^{\pi} \sin\omega t d(\omega t) = \frac{2I_m}{\pi}. \tag{2.10}$$

The presence of the filter capacitor C_f results in reduction in the ripple voltage across the output load resistance. Thus the current flowing through C_f is given by [15]

$$i_{Cf} \approx i_{D1} - I_o = \begin{cases} I_o(\pi \sin\omega t - 1), & \text{for} \quad 0 < \omega t \leq \pi \\ -I_O & \text{for} \quad \pi < \omega t \leq 2\pi. \end{cases} \tag{2.11}$$

.

2.4 Frequency-domain Analysis

In this section, further analysis in the frequency-domain under steady-state is performed on the SRC and various circuit parameters namely, current, voltage, voltage gain, input impedance, are determined. The frequency-domain analysis is helpful in its approach towards lower order systems providing simple analytical equations in terms of the circuit parameters. It also assists in understanding the circuit behaviour for variation in these parameters. A complete analysis of the converter in frequency-domain can be made by considering the inverter, resonant, and rectifier sections independently [1]. The parameters of the SRC are re-stated as follows. The angular resonant frequency

$$\omega_o = \frac{1}{\sqrt{LC}}, \tag{2.12}$$

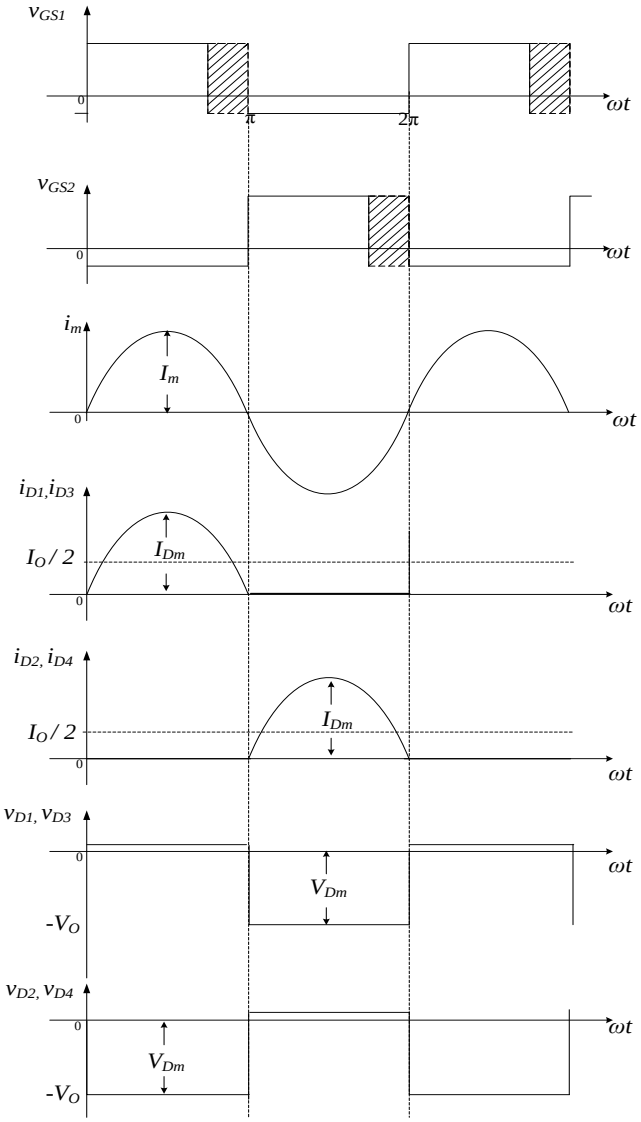

Figure 2.5: Voltage and current waveforms of the bridge rectifier diodes.

characteristic impedance

$$Z_o = \sqrt{\frac{L}{C}} = \omega_o L = \frac{1}{\omega_o C}, \tag{2.13}$$

loaded quality factor

$$Q_L = \frac{\omega_o L}{R} = \frac{1}{\omega_o C R} = \frac{Z_o}{R} = \frac{\sqrt{\frac{L}{C}}}{R}, \tag{2.14}$$

unloaded quality factor

$$Q_o = \frac{\omega_o L}{r} = \frac{1}{\omega_o C r} = \frac{Z_o}{r}, \tag{2.15}$$

where

$$R = R_e + r \qquad \text{and} \qquad r = r_{DS} + r_L + r_C. \tag{2.16}$$

The inductive reactance $X_L = \omega_o L$ and capacitive reactance is $X_C = \frac{1}{\omega_o C}$.

2.4.1 Input Impedance

The input impedance of the series resonant circuit is expressed as

$$\begin{aligned} Z &= R + X_L + X_C \\ &= R + j\left(\omega L - \frac{1}{\omega C}\right) = R\left[1 + j\frac{\omega L}{R}\left(1 - \frac{1}{\omega LC}\right)\right] \\ &= R\left[1 + jQ_L\left(\frac{\omega}{\omega_o} - \frac{\omega_o}{\omega}\right)\right] \end{aligned} \tag{2.17}$$

where

$$|Z| = R\sqrt{1 + {Q_L}^2\left(\frac{\omega}{\omega_o} - \frac{\omega_o}{\omega}\right)^2} = Z_O\sqrt{\left(\frac{R}{Z_O}\right)^2 + \left(\frac{\omega}{\omega_o} - \frac{\omega_o}{\omega}\right)^2}, \tag{2.18}$$

$$\psi = \arctan\left[Q_L\left(\frac{\omega}{\omega_o} - \frac{\omega_o}{\omega}\right)\right]. \tag{2.19}$$

From equation (2.18), it can be observed that, as the switching frequency f approaches f_o, the input impedance Z becomes equal to R, since the reactive effect offered by L and C will be cancelled. For all values of input impedance below f_o, the capacitive reactance is dominant and the circuit offers a capacitive load, Similarly, for values of impedance above f_o, the load becomes inductive in nature. At the resonant frequency, the capacitive and inductive reactances are in quadrature cancelling out one another. At this instant, the current is resisted only by the resistance of the converter. This effect is clearly depicted in Figure 2.6 which shows variaton of input impedance for different values of normalized switching frequency and R/Z_O.

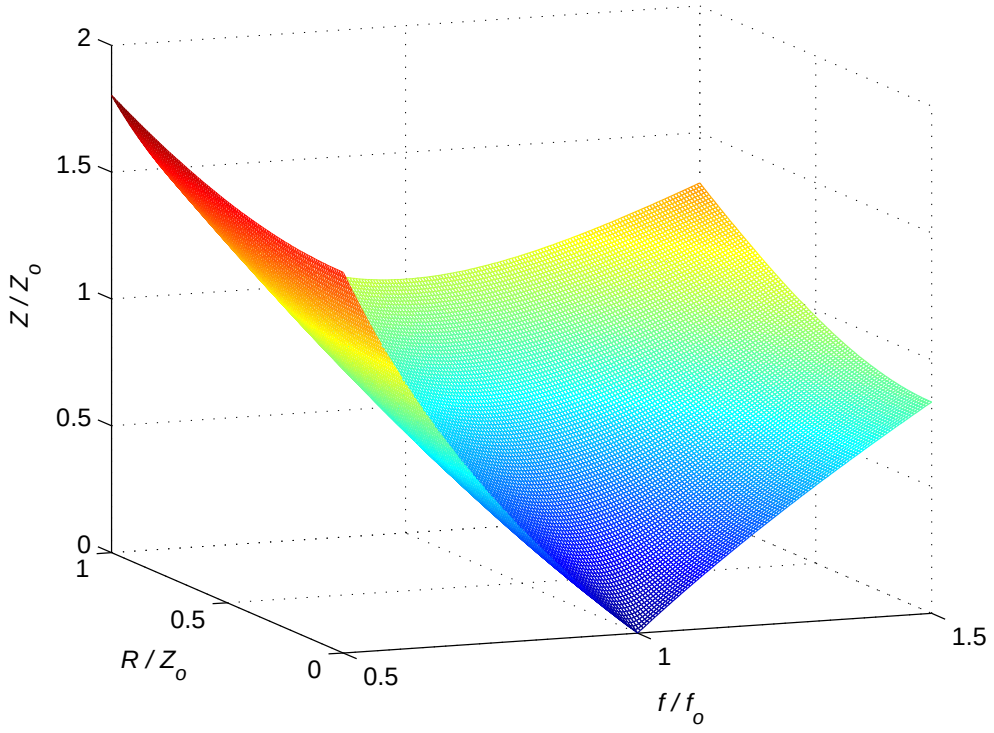

Figure 2.6: Variation of Z/Z_o as a function of f/f_o and R/Z_o

2.4.2 Short-circuit and Open-circuit Operation

The current i_m flowing through the series resonant circuit can be expressed as

$$I_m = \frac{V_m}{Z} = \frac{2V_I}{\pi Z}$$
$$= \frac{2V_I}{\pi R\sqrt{1 + {Q_L}^2\left(\frac{\omega}{\omega_o} - \frac{\omega_o}{\omega}\right)^2}}. \tag{2.20}$$

As can be seen from the above expression, as $\omega \to \omega_o$, $Z \to R$, where $R = r + R_L$. At resonant frequency, if the load is short-circuited, i.e., when $R_L = 0$, the total resistance offered to the current will be only by the esr r of the components. This results in the flow of very high current through the circuit components. For example, for $V_I = 270$ V and $r = 1.8\ \Omega$, then $I_m \approx 96$ A. This heavy current results in high amount of losses in the passive components and causes very high current stresses on the switches resulting in a catastrophic failure of the converter. Therefore,

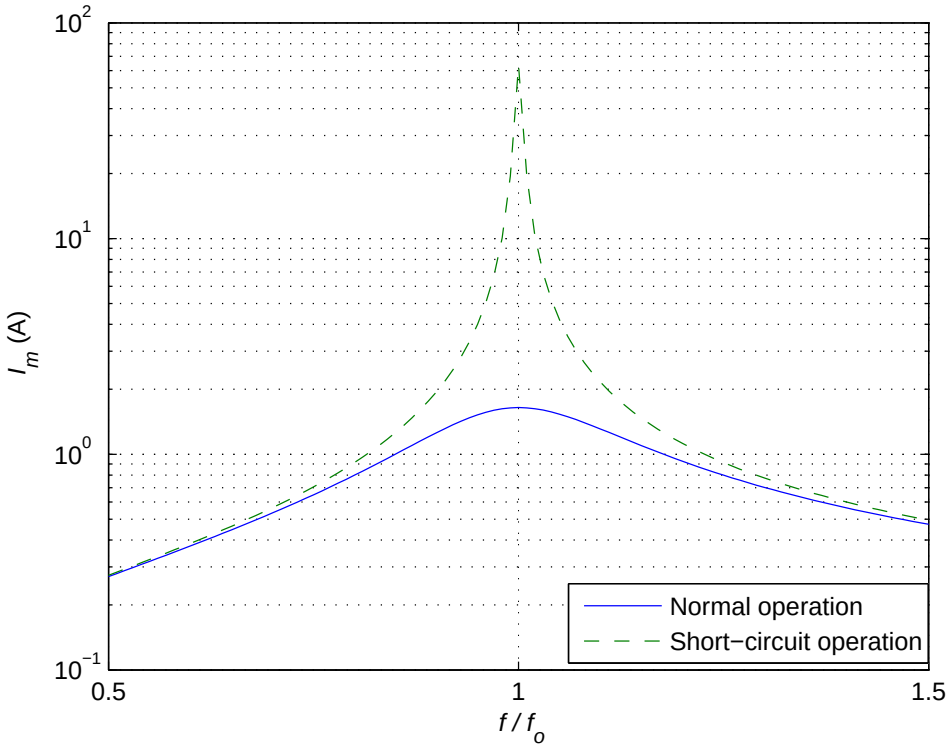

Figure 2.7: Variation of I_m as a function of f/f_o at normal and short-circuit operation.

short-circuit operation of SRC should be completely avoided when operating the converter close to resonant frequency. Similarly, the converter can operate safely at all frequencies when the output is open-circuited except at resonant frequency. The variation of I_m with respect to normalised switching frequency is shown in Figure 2.7.

2.4.3 Voltage Transfer Function

The voltage transfer function of the SRC can be calculated by considering the transfer functions of three cascaded stages of the converter namely, half-bridge inverter, resonant circuit and the full-bridge rectifier [15]. The voltage transfer function of the switching part will be the ratio of the square-wave voltage produced across S_2 and

the DC input voltage V_I given by

$$M_{Vs} = \frac{V_{S_{rms}}}{V_I}. \tag{2.21}$$

The rms value of V_s is given by

$$V_{S_{rms}} = \frac{\sqrt{2}V_I}{\pi}, \tag{2.22}$$

$$M_{Vs} = \frac{\sqrt{2}}{\pi} = 0.45. \tag{2.23}$$

The resonant current i_m is sinusoidal due to high Q_L of the inductor L. Therefore, the resonant circuit delivers maximum power when i_m is in phase with the fundamental component v_{s1} of the inverter output. The voltage transfer function M_{Vr} of the resonant circuit can be derived as follows.

$$V_R = V_{Srms}\frac{R}{R + X_L + X_C},$$

where $R = r + Re$.

$$M_{Vr} = \frac{V_R}{V_{Srms}} = \frac{R}{R + X_L + X_C} = \frac{R}{R + j\left(\omega L - \frac{1}{\omega C}\right)}$$

$$= \frac{R}{R\left[1 + j\frac{\omega_o L}{R}\left(\frac{\omega}{\omega_o} - \frac{1}{LC\omega}\right)\right]} = \frac{1}{\left[1 + jQ_L\left(\frac{\omega}{\omega_o} - \frac{\omega_o}{\omega}\right)\right]}, \tag{2.24}$$

$$|M_{Vr}| = \frac{1}{\sqrt{1 + {Q_L}^2\left(\frac{\omega}{\omega_o} - \frac{\omega_o}{\omega}\right)^2}}, \tag{2.25}$$

$$\psi = -\arctan\left[Q_L\left(\frac{\omega}{\omega_o} - \frac{\omega_o}{\omega}\right)\right]. \tag{2.26}$$

For a lossy converter, M_{Vr} can be modified to accommodate the efficiency η_I of the switching network. Equation (2.25) can be re-written as

$$|M_{Vr}| = \frac{\eta_I}{\sqrt{1 + {Q_L}^2\left(\frac{\omega}{\omega_o} - \frac{\omega_o}{\omega}\right)^2}}. \tag{2.27}$$

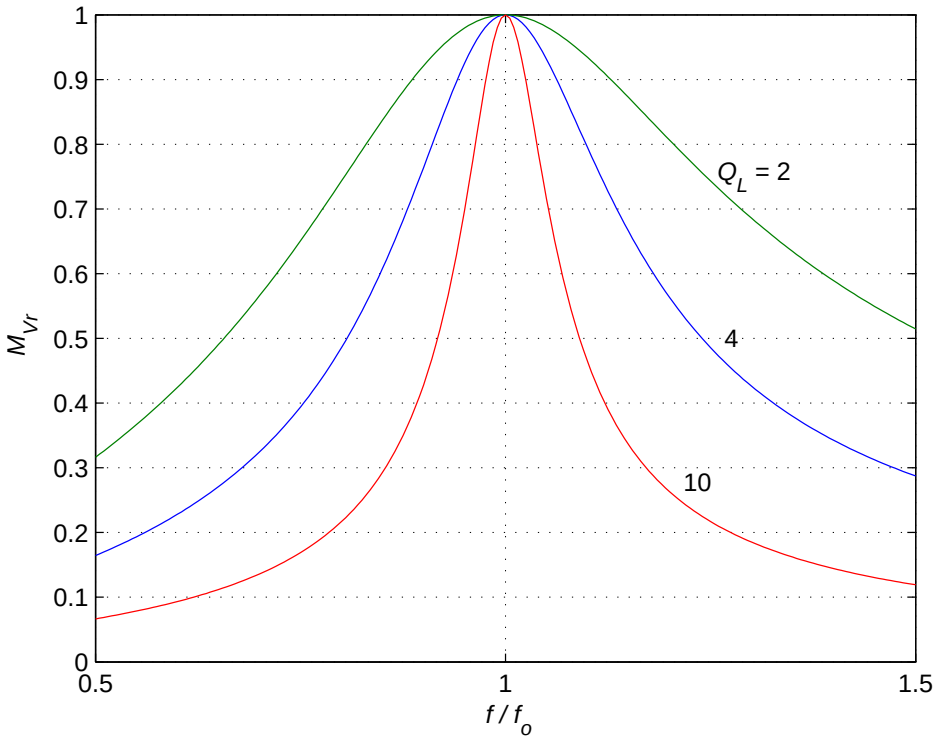

Figure 2.8: Variation of M_{Vr} as a function of f/f_o and Q_L

Th variation of M_{Vr} with respect to f/f_o and Q_L is depicted in Figure 2.8. It can be observed that the resonant circuit offers unity gain when f is equal to the f_o. At all other frequencies, the voltage gain is less than unity. Hence, the SRC is similar to a DC-DC buck converter.

The voltage transfer function of the full-bridge rectifier is provided in [15],

$$M_{VR} = \frac{V_o}{V_{Rrms}} = \frac{\pi}{2\sqrt{2}\left[1 + \frac{2V_F}{V_o} + \frac{\pi^2 R_F}{2R_L} + \frac{r_{Cf}}{R_L}\left(\frac{\pi^2}{8} - 1\right)\right]}, \tag{2.28}$$

where V_F and R_F are the forward voltage and on-state resistance of the diode respectively, r_{Cf} is the esr of the filter capacitor. From equations (2.23),(2.25), and (2.28), the voltage transfer function of the SRC M_V is expressed as

$$M_V = M_{Vs} M_{Vr} M_{VR} \tag{2.29}$$

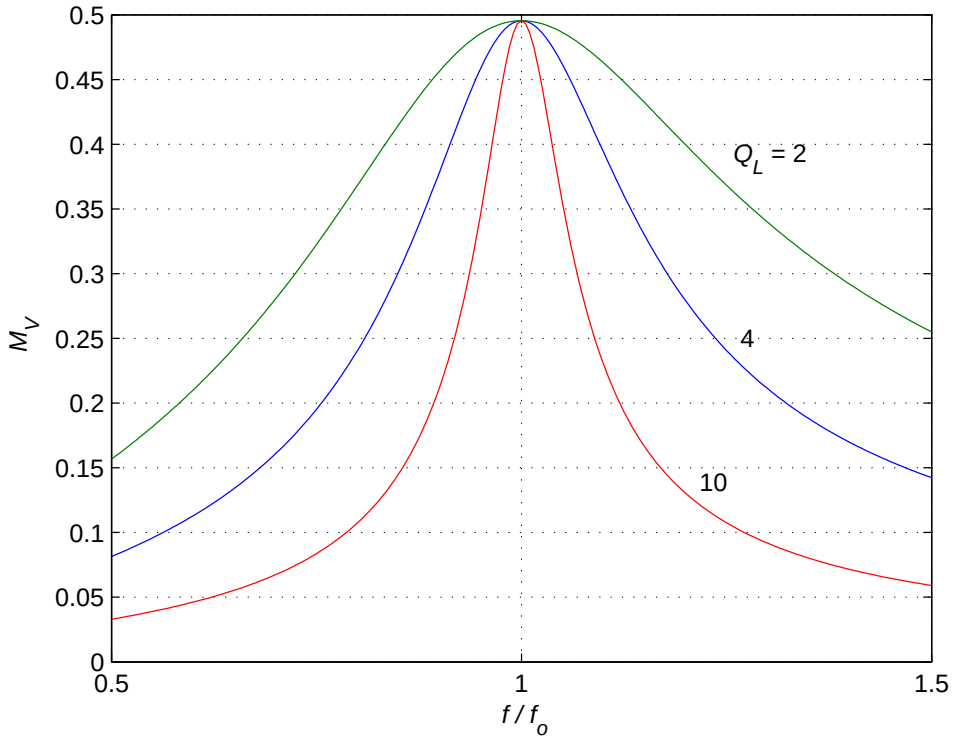

Figure 2.9: Variation of M_V as a function of f/f_o and Q_L.

$$M_V = \frac{1}{2\sqrt{1 + {Q_L}^2 \left(\frac{\omega}{\omega_o} - \frac{\omega_o}{\omega}\right)^2} \left[1 + \frac{2V_F}{V_o} + \frac{\pi^2 R_F}{2R_L} + \frac{r_{Cf}}{R_L}\left(\frac{\pi^2}{8} - 1\right)\right]}. \tag{2.30}$$

The variation of input-to-output voltage transfer function M_V with respect to normalized switching frequency f/f_o for different values of Q_L is shown in Figure 2.9. The range of output is limited to $0.5V_I$ due to the action of the bridge rectifier.

2.4.4 Current and Voltage Stresses

The alternate turn-on and turn-off of the MOSFETs causes a voltage V_I to appear across the S_2. Hence, the peak voltage across S_2 is equal to the DC input voltage

$$V_{SM} = V_I \tag{2.31}$$

The switches should be capable of withstanding very high currents under short-circuit situations, especially when the switching frequency approaches resonant frequency of

the converter. The peak switch current or the maximum amplitude of the resonant current through the switches is

$$I_{SM} = I_{m_{max}} = \frac{2V_I}{\pi r}, \tag{2.32}$$

where $r = r_{DS} + r_L + r_C$. The sinusoidal nature of the resonant current i_m causes a sinusoidal voltage V_L to appear across the resonant inductor L. The peak value of voltage V_{Lm} is given by

$$\begin{aligned} V_{Lm} &= I_m X_L = I_m \omega L \\ &= \frac{2V_I \omega L}{\pi R \sqrt{1 + {Q_L}^2 \left(\frac{\omega}{\omega_o} - \frac{\omega_o}{\omega}\right)^2}}. \end{aligned} \tag{2.33}$$

Similarly, the peak value of voltage across the resonant capacitor C is given by

$$\begin{aligned} V_{Cm} &= I_m X_C = \frac{I_m}{\omega C} \\ &= \frac{2V_I}{\omega C \pi R \sqrt{1 + {Q_L}^2 \left(\frac{\omega}{\omega_o} - \frac{\omega_o}{\omega}\right)^2}}. \end{aligned} \tag{2.34}$$

The variation of V_{Lm} and V_{Cm} with normalized switching frequency are shown in Figures 2.10 and 2.11. It can be seen that at frequencies close to the resonant frequency, the voltage reaches very high values when the load resistance is short-circuited.

The current-driven bridge rectifier will have maximum stresses that depend on the output voltage V_O. The peak reverse voltage stress across the diodes is expressed as

$$V_{DM} = V_O. \tag{2.35}$$

The peak current flowing through the diodes can be obtained using equation (2.10) is given by

$$I_{DM} = I_m = \frac{\pi I_O}{2}. \tag{2.36}$$

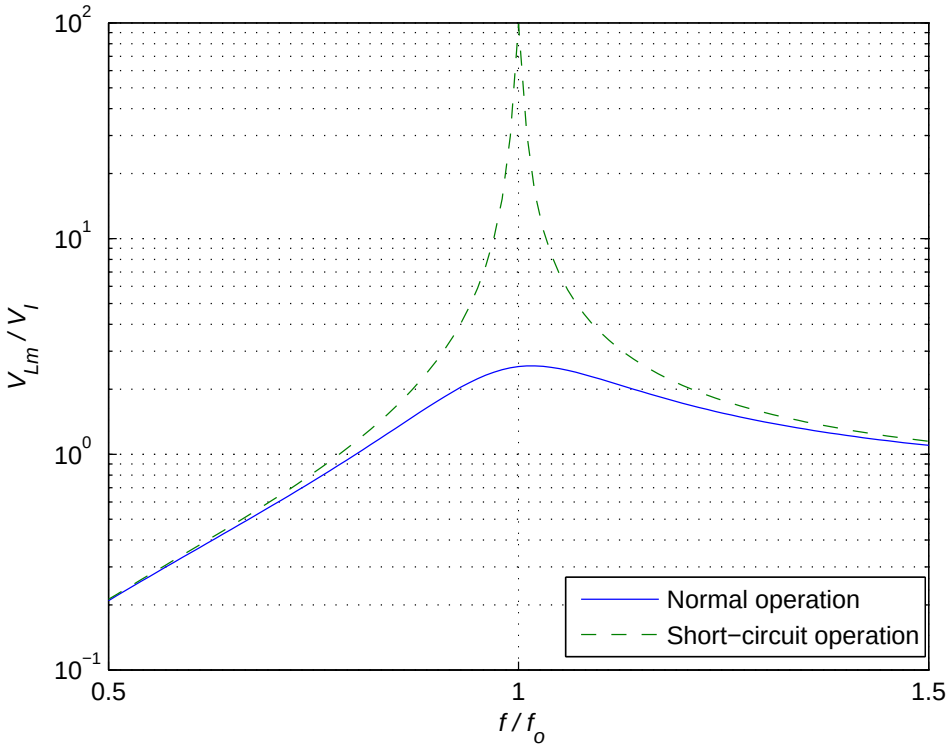

Figure 2.10: Variation of V_{Lm}/V_I as a function of f/f_o for normal and short-circuit operation.

2.4.5 Efficiency

The flow of current through the circuit components causes conduction losses in them due to the presence of the resistances r_{DS}, r_C, r_L, R_F and r_{Cf} in the switches, resonant capacitor, resonant inductor, diodes and filter capacitor respectively. Thus, the efficiency of the converter is reduced. The efficiency η of the SRC is derived as follows. Current through the MOSFET switches causes a power loss

$$P_{rDS} = \frac{I_m^2 r_{DS}}{4}. \tag{2.37}$$

The r_L of the inductor dissipates power which is given by

$$P_{rL} = \frac{I_m^2 r_L}{2}. \tag{2.38}$$

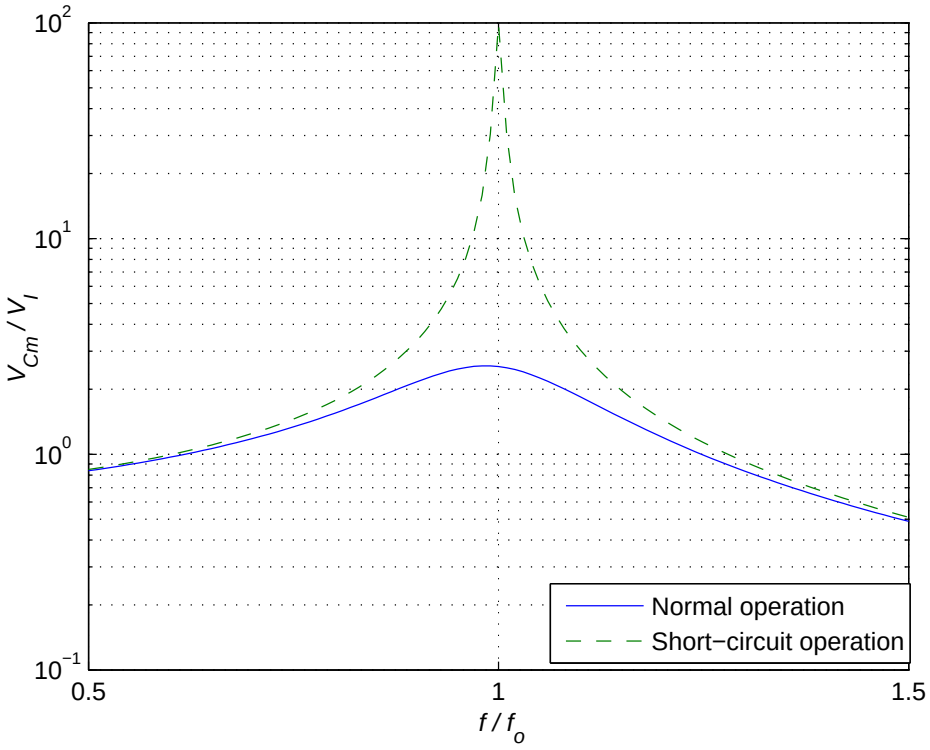

Figure 2.11: Variation of V_{Cm}/V_I as a function of f/f_o for normal and short-circuit operation.

Similarly, the esr r_C of the capacitance produces losses given by

$$P_{rC} = \frac{I_m^2 r_C}{2}. \tag{2.39}$$

The total losses in the series resonant inverter is given by

$$P_r = 2P_{rDS} + P_{rC} + P_{rL} = \frac{I_m^2(r_{DS} + r_L + r_C)}{2} = \frac{I_m^2 r}{2}. \tag{2.40}$$

Therefore, the efficiency of the series resonant inverter is expressed as

$$\eta_I = \frac{P_{Re}}{P_I} = \frac{P_{Re}}{P_{Re} + P_r} = \frac{I_m^2 R_e}{I_m^2 (R_e + r)} \tag{2.41}$$

where R_e is the effective resistance offered by the bridge-rectifier to the resonant current i_m and P_{Re} is the output power of series resonant inverter. R_e is given by

$$R_e = \frac{8R_L}{\pi^2}\left[1 + \frac{2V_F}{V_O} + \frac{\pi^2 R_F}{4R_L} + \frac{r_{Cf}}{R_L}\left(\frac{\pi^2}{8} - 1\right)\right] = \frac{8R_L}{\pi^2 \eta_R}. \tag{2.42}$$

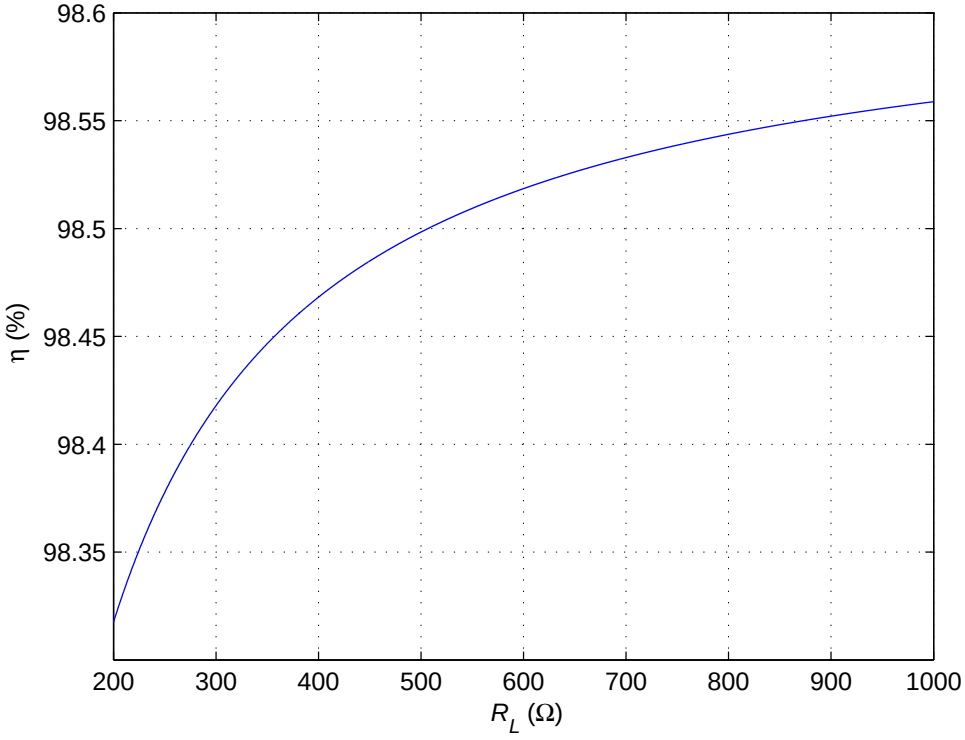

Figure 2.12: Variation of η of SRC with load resistance R_L.

The efficiency of the bridge-rectifier is derived in [15]. It is expressed as

$$\eta_R = \frac{8R_L}{\pi^2 R_e}. \tag{2.43}$$

The total efficiency of the SRC η is expressed as the product of the efficiencies of the series resonant inverter η_I and the bridge rectifier η_R

$$\eta = \eta_I \eta_R. \tag{2.44}$$

Figure 2.12 depicts the efficiency of the SRC with variation in the load resistance. It can be observed that the efficiency increases with higher values of load resistance R_L.

3 Parallel and Series-parallel Resonant Converter Configurations

The operation and functional characteristics of series resonant converters (SRC) have been discussed in the previous chapters. The present chapter explains briefly about the parallel resonant (PRC) and series-parallel resonant converters (SPRC). Similar to SRC, the impedance equations that help in determining short-circuit and open-circuit conditions of the resonant circuit are provided. Using a design example, the efficiency plots of the PRC and SPRC are shown and briefly compared. The parameters that are used in the analysis, which are relevant to all resonant converters, are the resonant frequency f_O, characteristic impedance Z_o, and quality factor Q_L given by

$$f_o = \frac{1}{\sqrt{LC}}, \tag{3.1}$$

$$Z_o = \sqrt{\frac{L}{C}}, \tag{3.2}$$

$$Q_L = \frac{Z_o}{R}, \tag{3.3}$$

where L and C are resonant inductance and capacitance, respectively, and R is the ac load resistance.

3.1 Parallel Resonant Converter

Figure 3.1 shows the circuit of a half-bridge parallel resonant converter. The half-bridge PRC is obtained by cascading a half-bridge parallel resonant inverter (PRI) with half-wave voltage-driven rectifier. The principle of operation of PRC is explained in [16], [19]. If the Q_L of the resonant circuit is high and f is close to f_o, then the output of the PRI is considered as a sinusoidal voltage source. Power from source to the load is delivered by tapping the resonant voltage appearing across the capacitor of the PRI. Usually, a coupling capacitor C_C is connected in series with L to protect the converter from DC short-circuit and the entire square wave voltage applied by the

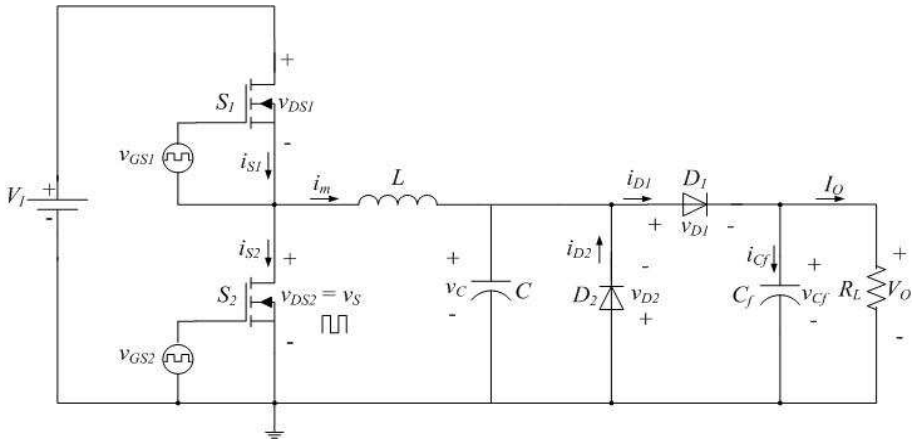

Figure 3.1: Basic circuit diagram of parallel resonant converter.

half-bridge connected MOSFET network appears across the inductor L and hence, the current is limited by its impedance. Therefore, the PRC is inherently short-circuit protected at all frequencies. The impedance of the parallel resonant circuit is given by

$$Z = \frac{1}{\frac{1}{R} + j\left(\omega C - \frac{1}{\omega L}\right)}, \tag{3.4}$$

$$Z = |Z|e^{j\psi}, \tag{3.5}$$

where

$$|Z| = \frac{R}{\sqrt{1 + Q_L^2\left(\frac{\omega}{\omega_o} - \frac{\omega_o}{\omega}\right)^2}}, \tag{3.6}$$

and

$$\psi_Z = -\arctan\left(\frac{\omega}{\omega_o} - \frac{\omega_o}{\omega}\right). \tag{3.7}$$

At $f = f_o$, the input impedance will be equal to only the parasitic resistances r and I_m will be very high. But when the load is open circuited i.e., $R_L = \infty$, then, it can lead to an excessive current through the resonant circuit and the transistors which results in very high voltage across the resonant L and C. The amplitude I_m of current

i_m through the resonant circuit at $f = f_o$ is given by

$$I_m = \frac{2V_I}{\pi r}, \tag{3.8}$$

and the peak values of voltage across the resonant L and C are similar to those given Chapter 2 for SRC. Consider a PRC operating at $V_I = 250$ V, $Z_o = 300\ \Omega$, $r = 1\ \Omega$, then $I_m = 159$ A and $V_{Cm} = V_{Lm} = 47.7$ kV. Thus the operation at resonant frequency must be avoided, especially at $R_L = \infty$. However, for applications like electronic ballasts, this surge in voltage and current is used to start the lamp. The efficiency of the PRC can be obtained in a manner similar to that of the SRC. Since the PRC is a combination of the parallel resonant inverter (PRI) with a half-wave rectifier connected across the output of the PRI, the efficiency of the PRC η_P can be expressed as [15],

$$\eta_P = \eta_{PRI}\eta_R, \tag{3.9}$$

where η_{PRI} is the efficiency of the parallel resonant inverter and η_R is the efficiency of the half-wave rectifier circuit. η_P is dependent on Q_L and reduces with increase in load as shown in Figure 3.2. The efficiency is calculated for a transformerless parallel resonant converter having the following specifications: $R_L = 200\ \Omega$ to 1 kΩ, $V_I = 200$ V, $V_O = 100$ V, $P_{Omax} = 50$ W, $L_f = 1$ mH and resonant frequency is $f_o = 115$ kHz and switching frequency at full load is $f = 120$ kHz.

The PRC inclusive of the output filter inductor is well suited for applications that need low output voltage and high output current [18]. In a very narrow frequency range, the PRC is able to regulate output voltage from no load to full load conditions which is not possible in the case of SRC. Also, the converter can operate both as buck and boost systems at higher frequencies with the inclusion of a transformer and by varying the turns ratio. A major disadvantage of the PRC is that the current through the switches and resonant inductance and capacitance is independent of the variation in load demands. Also, PRC develops very high circulating currents with increase

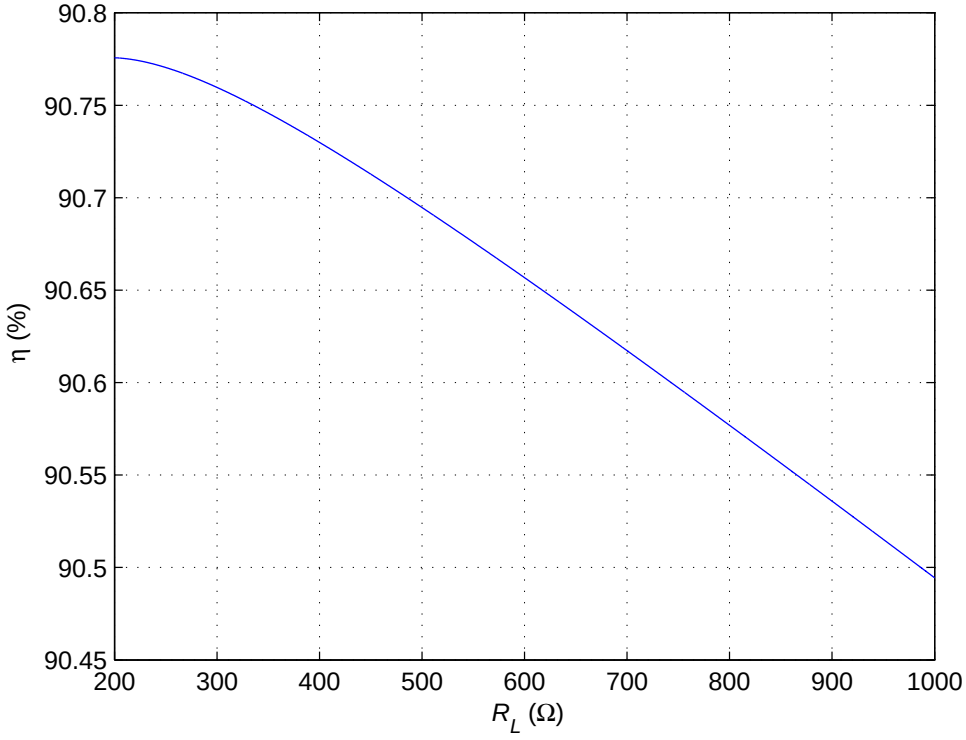

Figure 3.2: Variation of efficiency η as a function of load resistance R_L of PRC.

in input voltage making it less efficient for applications been driven by large supply voltages.

3.2 Series-parallel Resonant Converter

Figure 3.3 shows the circuit of series-parallel resonant converter (SPRC). The principle of operation of SPRC is explained in [16], [17]. The SPRC behaves as SRC at full load condition and as PRC at light load conditions. It eliminates few of the most important drawbacks of the pure SRC and pure PRC namely, lack of no load regulation of the SRC and circulating current being independent of the load in the PRC at full loads. SPRC also provides zero-current switching (ZCS) and zero-voltage switching (ZVS) of the converter switches. The switching scheme is designed to minimize the switching losses and this design is very helpful at higher switching frequencies. From the circuit

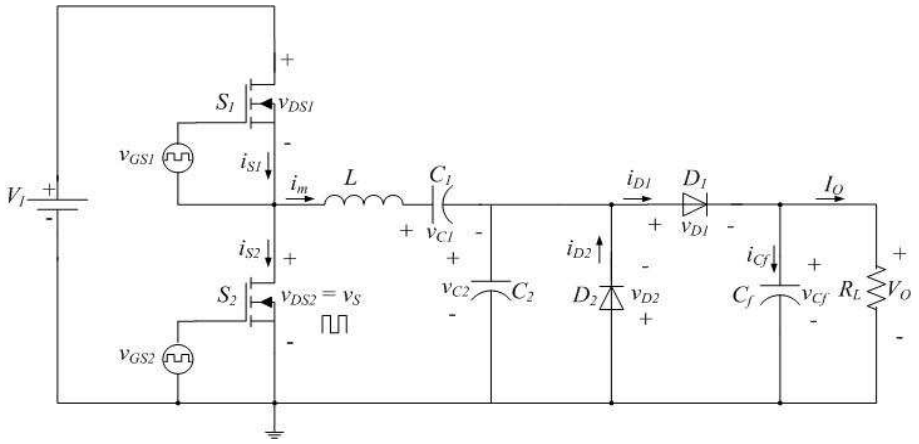

Figure 3.3: Basic circuit diagram of series-parallel resonant converter.

construction, it can be seen that if capacitor C_2 is zero then the SPRC becomes SRC and if the capacitor is replaced by a dc-blocking capacitor and C_2 added in parallel, then the SPRC becomes a PRC. The series capacitance C_1, makes the equivalent tank capacitance smaller and also reduces the characteristic impedance of the resonant circuit and this is required in order to suppress the circulating current.

The input impedance of the series-parallel resonant circuit [16] is given by

$$Z = \frac{R(1+A)\left[1-\left(\frac{\omega}{\omega_o}\right)^2\right] + j\frac{1}{Q_L}\left(\frac{\omega}{\omega_o} - \frac{\omega_o}{\omega}\frac{A}{A+1}\right)}{1 + jQ_L\left(\frac{\omega}{\omega_o}\right)(1+A)} \tag{3.10}$$

$$Z = |Z|e^{j\psi}, \tag{3.11}$$

where

$$|Z| = R\sqrt{\frac{(1+A)^2\left[1-\left(\frac{\omega}{\omega_o}\right)^2\right]^2 + \frac{1}{Q_L^2}\left[\frac{\omega}{\omega_o} - \frac{\omega_o}{\omega}\frac{A}{A+1}\right]^2}{1+\left[Q_L\left(\frac{\omega}{\omega_o}\right)(1+A)\right]^2}}, \tag{3.12}$$

$$\psi = \arctan\left\{\frac{1}{Q_L}\left(\frac{\omega}{\omega_o} - \frac{\omega_o}{\omega}\frac{A}{A+1}\right) - Q_L\left(\frac{\omega}{\omega_o}\right)(1+A)^2\left[1-\left(\frac{\omega}{\omega_o}\right)^2\right]\right\} \tag{3.13}$$

and

$$A = C_2/C_1.$$

The maximum switch current I_m also equal to the maximum value of the current through the resonant circuit and given by

$$I_{SM} = I_m$$
$$= \frac{2V_I}{\pi R_{min}} \sqrt{\frac{1 + \left[Q_L \left(\frac{\omega}{\omega_o}\right)(1+A)^2\right]}{(1+A)^2 \left[1 - \left(\frac{\omega}{\omega_o}\right)^2\right]^2 + \frac{1}{Q_L^2}\left[\frac{\omega}{\omega_o} - \frac{\omega_o}{\omega}\frac{A}{A+1}\right]^2}}. \tag{3.14}$$

The converter is not safe under short-circuit and the open-circuit conditions at two different frequencies determined by the resonant components. At $R_L = 0$, the capacitor C_2 is short-circuited and the resonant circuit consists of L and C_1. If the f equals f_{rs}, which is the resonant frequency of the new $L - C_1$ circuit, the magnitude of the current through the switches and that of the $L - C_1$ circuit is

$$I_m = \frac{2V_I}{\pi r}. \tag{3.15}$$

This current may become excessive, thus causing damage to the circuit. If f_{rs} is far away from the switching frequency f, I_m is limited by the reactance of the resonant circuit. On the other hand, if $R_L = \infty$, then the resonant circuit comprises of L and a series combination of C_1 and C_2. So, as f approaches f_{rp}, the resonant frequency of L-C_1-C_2 circuit, again, the current increases to a very large value as given above, causing damage to the converter components.

The voltage across the resonant components V_{Lm}, V_{C1m}, V_{C2m} are given by

$$V_{Lm} = \omega L I_m, \tag{3.16}$$

$$V_{C1m} = \frac{I_m}{\omega C_1}, \tag{3.17}$$

$$V_{C2m} = \frac{2V_I}{\pi \sqrt{(1+A)^2 \left[1 - \left(\frac{\omega}{\omega_o}\right)^2\right]^2 + \frac{1}{Q_L^2}\left[\frac{\omega}{\omega_o} - \frac{\omega_o}{\omega}\frac{A}{A+1}\right]^2}}. \tag{3.18}$$

The efficiency of the SPRC η_{SP} can be obtained by considering the efficiencies of the series-parallel resonant inverter (SPRI) η_{SPRI} and the half-wave rectifier η_R.

$$\eta_{SP} = \eta_{SPRI}\eta_R. \tag{3.19}$$

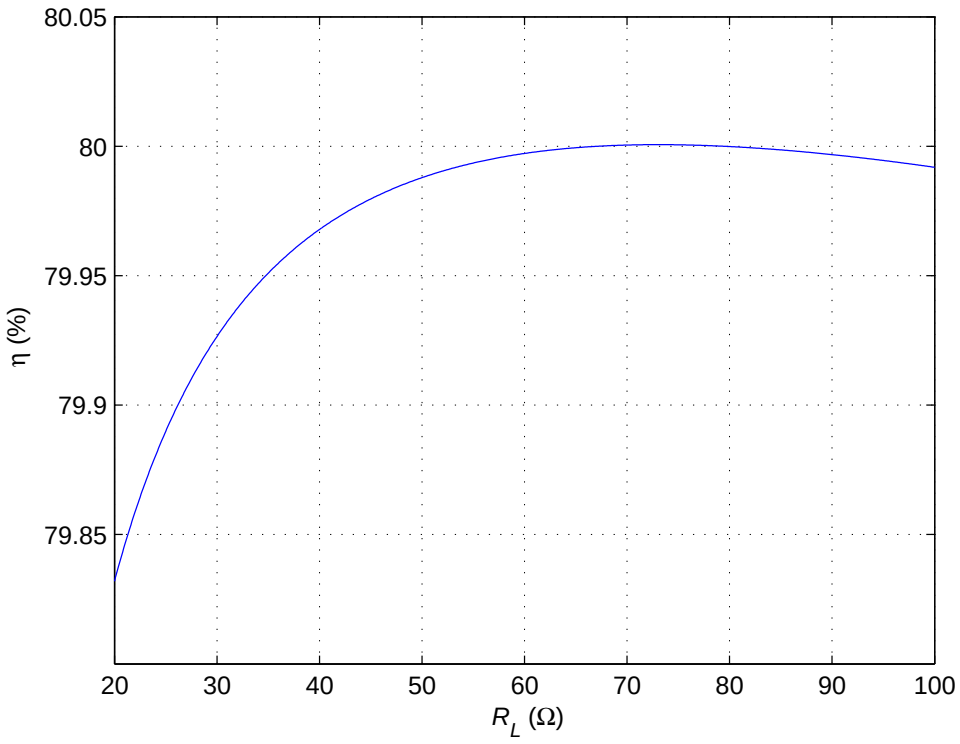

Figure 3.4: Variation of efficiency η as a function of load resistance R_L of SPRC.

The efficiency plot of a SPRC is as shown in Figure 3.4. The efficiency is calculated for a transformerless series-parallel resonant converter having the following specifications: $R_L = 20\ \ \Omega$ to $100\ \ \Omega$, $V_I = 250\ \ \text{V}$, $V_O = 40\ \ \text{V}$, $P_{Omax} = 80\ \ \text{W}$, $f_o = 100\ \ \text{kHz}$ and f at full load $= 80\ \ \text{kHz}$.

Disadvantage of the SPRC is that the converter has a third order resonant tank circuit, which makes it difficult to apply certain analytical techniques for its modeling since it increases the complexity of the circuit. The converter will exhibit two resonant frequencies f_{rs} and f_{rp}. Short-circuit and open-circuit operation of the converter must be avoided at these frequencies to avoid flow of excessive currents.

4 Small-signal Modeling of Series Resonant Converter

4.1 Analysis of the Non-linear State Equations

The circuit diagram of the SRC is as shown in Figure 4.1. V_I represents the input voltage and the switches are turned on for a duty cycle D. i_m is the current through the inductor having peak value I_m and V_m is the peak value of voltage across the capacitor C. The turn-on and turn-off of diodes of D_1, D_2, D_3, and D_4 enables in the rectification of the resonant current i_m and hence, delivering output voltage V_O across R_L. $|i_m|$ is the rectified current flowing into the output filter network. A current source i_o is considered at the output which acts as a current sink. This also enables us to obtain the output impedance transfer characteristics of the converter. The filter capacitor C_f gets charged to a value V_{Cf} due to the flow of current i_{Cf} through it. The equivalent series resistances r_s is the sum of the esr of the resonant elements L and C given by $r_s = r_L + r_C$. The switching frequency is represented as f_s in this analysis for the purpose of understanding.

Applying KVL to the resonant and rectifier networks, V_{AB} is expressed as,

$$V_{AB} = V_m + L\frac{dI_m}{dt} + \text{sgn}(i_m)V_O. \tag{4.1}$$

The current through C is given by

$$C\frac{dV_m}{dt} = I_m. \tag{4.2}$$

The current i_{Cf} flowing through C_f is

$$C_f\frac{dV_{C_f}}{dt} + \frac{V_O}{R_L} = |i_m| + i_o, \tag{4.3}$$

or

$$i_{Cf} = |i_m| + i_o - \frac{V_O}{R_L}. \tag{4.4}$$

The output rectifier-filter loop can be used to obtain the expression for output voltage V_O. Applying KVL to the output loop, we obtain

$$V_O = i_{Cf} r_{Cf} + V_{Cf},$$

Substituting (4.4) in V_O, we obtain

$$V_O = \left(|i_m| + i_o - \frac{V_O}{R_L}\right) r_{Cf} + V_{Cf},$$

$$V_O \left(1 + \frac{r_{Cf}}{R_L}\right) = (|i_m| + i_o) r_{Cf} + V_{Cf}, \tag{4.5}$$

$$V_O = (|i_m| + i_o) \frac{r_{Cf} R_L}{r_{Cf} + R_L} + V_{Cf} \frac{R_L}{r_{Cf} + R_L},$$

$$V_O = (|i_m| + i_o) r_o + V_{Cf} \frac{r_o}{r_{Cf}}, \tag{4.6}$$

where

$$r_o = \frac{r_{Cf} R_L}{r_{Cf} + R_L}.$$

4.2 Harmonic Approximation

From the above set of equations it can be said that the converter is characterized by three state variables and are energy storing quantities namely I_m, V_m and V_{Cf} [22]. These quantities are associated with the resonant inductance L, resonant capacitance C, and the filter capacitance C_f. These state-space variables can be expressed as

$$\vec{X} = \begin{bmatrix} I_m \\ V_m \\ V_{Cf} \end{bmatrix} \tag{4.7}$$

Voltage V_{AB}, the switch currents I_{S1}, I_{S2} are dependent on the duty cycle D and switching frequency f_s. It is observed that the capacitor voltage v_m and inductor current i_m are approximately sinusoidal due to the high quality factor of the resonant circuit. This enables us to approximate the magnitudes V_m and I_m by their fundamental terms using Fourier series expansion principle. In general, any periodically

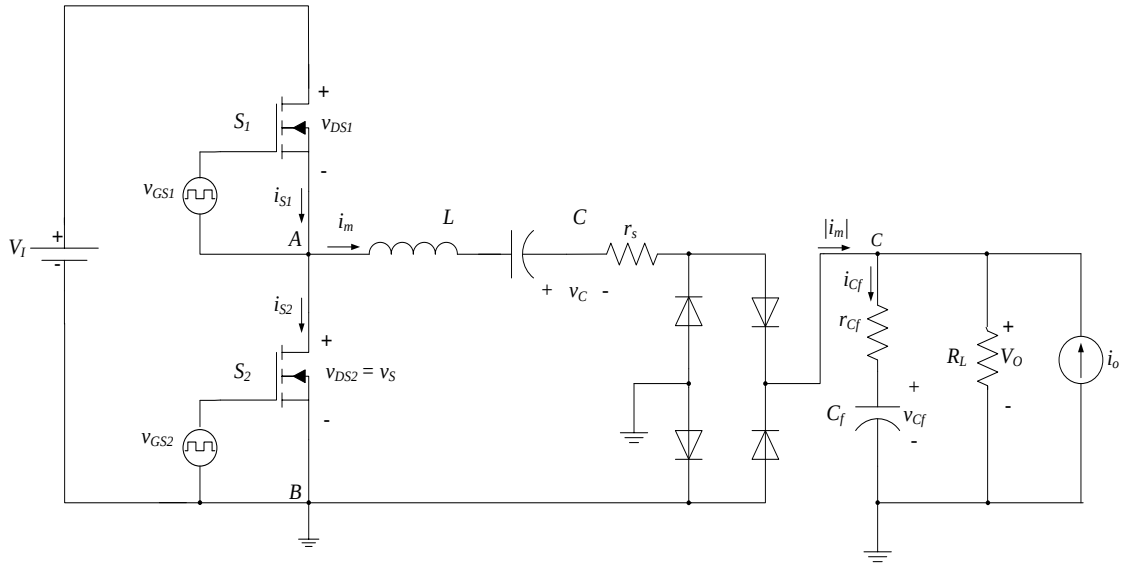

Figure 4.1: Circuit diagram of series resonant converter.

varying quantity $h(t)$ can be expressed as follows

$$h(t) = a_o + \sum[a_k \cos(k\omega_s t) + b_k \sin(k\omega_s t)] \tag{4.8}$$

Considering only the first harmonic ($k = 1$) and neglecting the fundamental and higher harmonics, we obtain

$$h(t) = a_1 \cos(\omega_s t) + b_1 \sin(\omega_s t) \tag{4.9}$$

Let $a_1 = H_c$ and $b_1 = H_s$, then

$$h(t) = H_c \cos(\omega_s t) + H_s \sin(\omega_s t), \tag{4.10}$$

where H_c corresponds to the sub-magnitude of the co-sinusoidal part of $h(t)$ and H_s represents the sub-magnitude of the sinusoidal part of $h(t)$.

This principle can be applied to the resonant voltage V_m and current I_m, to obtain

$$V_m(t) = V_C\cos(\omega_s t) + V_S\sin(\omega_s t), \tag{4.11}$$

$$I_m(t) = I_C\cos(\omega_s t) + I_S\sin(\omega_s t). \tag{4.12}$$

The quantities V_C, V_S, I_C, and I_S are slowly time varying and hence the steady-state dynamic equivalent model can be derived [23].

Differentiating equations (4.11) and (4.12) with respect to t, we obtain

$$\frac{dV_m}{dt} = \frac{dV_C}{dt}\cos(\omega_s t) - V_C\omega_s\sin(\omega_s t) + \frac{dV_S}{dt}\sin(\omega_s t) + V_S\omega_s\cos(\omega_s t), \tag{4.13}$$

$$\frac{dI_m}{dt} = \frac{dI_C}{dt}\cos(\omega_s t) - I_C\omega_s\sin(\omega_s t) + \frac{dI_S}{dt}\sin(\omega_s t) + I_S\omega_s\cos(\omega_s t). \tag{4.14}$$

Rearranging the non-linear state equations given in (4.1), (4.2), and (4.3), we obtain

$$L\frac{dI_m}{dt} = V_{AB} - V_m + \text{sgn}(i_m)V_O, \tag{4.15}$$

$$C\frac{dV_m}{dt} = I_m, \tag{4.16}$$

$$C_f\frac{dV_{Cf}}{dt} = |I_m| + i_o - \frac{V_O}{R_L}. \tag{4.17}$$

4.3 Derivation of Extended Describing Functions

The extended describing function (EDF) method provides a complete description about the behaviour of the converter due to small-signal changes in input voltage $\hat{v}_i$, variations in the switching frequency $\hat{f}_s$ and the duty-cycle $\hat{d}$. Now, the time varying quantities described in equations (4.15), (4.16) and, (4.17) needs to be expressed as functions in terms of the input and control variables. Let

$$V_{AB}(t) = f_1(D, V_I)\sin\omega_s t, \tag{4.18}$$

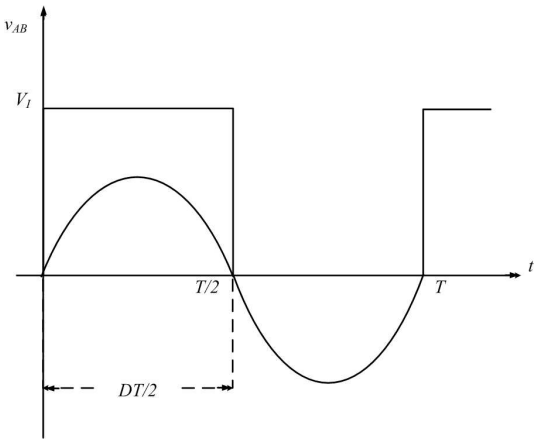

Figure 4.2: Square-wave voltage V_{AB}.

$$\mathrm{sgn}(I_m)V_O = f_2(I_S, I_C, V_{Cf})\mathrm{sin}\omega_s t + f_3(I_S, I_C, V_{Cf})\mathrm{cos}\omega_s t, \tag{4.19}$$

The functions f_1, f_2, f_3, and f_4 are called extended describing functions. They provide a relation between the variables that decide the operating point of the converter and the harmonics of the state variables $\vec{X}$ [23].

The square-wave $V_{AB}(t)$ shown in Figure 4.2 can be approximated in terms of sinusoidal quantity [21]. The Fourier expansion of $V_{AB}(t)$ can be derived as follows. The Fourier series expansion of a function f_n is given by

$$f_n = a_o + \sum_{n=1}^{\infty} \left[a_n \mathrm{cos}n\omega_s t + b_n \mathrm{sin}n\omega_s t\right], \tag{4.20}$$

where

$$a_o = \frac{1}{T}\int_0^T f_n(t)dt, \tag{4.21}$$

$$a_n = \frac{2}{T}\int_0^T f_n(t)\mathrm{cos}n\omega_s t dt, \tag{4.22}$$

$$b_n = \frac{2}{T}\int_0^T f_n(t)\mathrm{sin}n\omega_s t dt. \tag{4.23}$$

V_{AB} is an odd function, hence a_o and a_n are zero. Therefore,

$$b_n = \frac{2}{T}\int_0^T f_n(t)\sin\left(\frac{n\pi Dt}{T/2}\right)dt$$

$$= \frac{4}{T}\int_0^{DT/2} f_n(t)\sin\left(\frac{2n\pi t}{T}\right)dt = \frac{4V_I}{T}\Big[-\cos\frac{2n\pi t}{T}\frac{T}{2n\pi}\Big]_0^{DT/2}$$

$$= \frac{4V_I}{2n\pi}\left[1+\cos\left(\frac{2n\pi DT}{2T}\right)\right] = \frac{4V_I}{2n\pi}\left[1-\cos(n\pi D)\right],$$

where $f_n(t) = V_I$ for $t \leq DT/2$. The term $\cos n\pi D$ can be approximated to be equal to $(-1)^n$. Rewriting above expression in simple terms, we obtain

$$b_n = \frac{2V_I}{n\pi}\left[1-(-1)^n\right]. \tag{4.24}$$

Substituting equation (4.24) in equation (4.20), we get

$$f_n = \sum_{n=1}^{\infty}\frac{2V_I}{n\pi}\left[1-D(-1)^n\right]\sin\left(\frac{n\pi D}{2}\right). \tag{4.25}$$

Since only the first harmonic content is of prime importance for the extended describing function method, i.e., $n = 1$, then equation (4.25) can be expressed as

$$f_1 = \frac{2V_I}{\pi}\sin\left(\frac{\pi D}{2}\right), \tag{4.26}$$

i.e.,

$$V_{AB} = \frac{2V_I}{\pi}\sin\left(\frac{\pi D}{2}\right). \tag{4.27}$$

The functions f_2 and f_3 are dependent on the current flowing into the rectifier and the effective voltage appearing across the output. They can be represented as the rms values of the voltage appearing across the rectifier output terminals. In order to bring about the effect of the rectified current, they are expressed in terms of I_S, I_C, and I_P as,

$$f_2(I_S, I_C, V_{Cf}) = \frac{4}{\pi}V_{Cf}\frac{I_S}{I_P}, \tag{4.28}$$

and,

$$f_3(I_S, I_C, V_{Cf}) = \frac{4}{\pi} V_{Cf} \frac{I_C}{I_P}, \tag{4.29}$$

where, the factor $4V_{Cf}/\pi$ is equal to the amplitude of the fundamental component of voltage appearing across the rectifier input terminals. I_P represents the magnitude of complex quantities I_S and I_C where

$$I_P = \sqrt{{I_S}^2 + {I_C}^2}.$$

Substituting (4.27),(4.28), and (4.29) in (4.15)

$$L\left(\frac{dI_C}{dt}\cos\omega_s t - I_C\omega_s \sin\omega_s t + \frac{dI_S}{dt}\sin\omega_s t - I_S\omega_s\cos\omega_s t\right)$$

$$= \frac{2}{\pi}V_I \sin(\frac{\pi D}{2}) - r_s(I_C\cos\omega_s t + I_S\sin\omega_s t) - (V_C\cos\omega_s t + V_S\sin\omega_s t) - \frac{4V_{Cf}}{\pi I_P}(I_C\cos\omega_s t + I_S\sin\omega_s t). \tag{4.30}$$

Similarly, substituting the E.D functions in (4.16) and (4.17)

$$C\left(\frac{dV_C}{dt}\cos\omega_s t - V_C\omega_s\sin\omega_s t + \frac{dV_S}{dt}\sin\omega_s t + V_S\omega_s\cos\omega_s t\right)$$

$$= I_C\cos\omega_s t + I_S\sin\omega_s t, \tag{4.31}$$

and

$$C_f\frac{dV_{Cf}}{dt} = \frac{2}{\pi}I_P + i_o - \frac{V_O}{R_L}, \tag{4.32}$$

where $|i_m|$ is expressd as the rms value of the output current flowing from the rectifier output terminals. Equating the sine and cosine terms in the above set of equations, we obtain

$$L\left(\frac{dI_C}{dt} + I_S\omega_s\right) = -r_S I_C - V_C - \frac{4V_{Cf}I_C}{\pi I_P}, \tag{4.33}$$

$$L\left(\frac{dI_S}{dt} - I_C\omega_s\right) = \frac{2V_I}{\pi}\sin\left(\frac{\pi D}{2}\right) - r_S I_S - V_C - \frac{4V_{Cf}I_S}{\pi I_P}, \tag{4.34}$$

$$C\left(\frac{dV_C}{dt} + \omega_s V_S\right) = I_C, \tag{4.35}$$

$$C\left(\frac{dV_S}{dt}+\omega_s V_C\right)=I_S, \tag{4.36}$$

$$C_f\frac{dV_{Cf}}{dt}=\frac{2I_P}{\pi}+i_o-\frac{V_O}{R_L}. \tag{4.37}$$

Equations (4.33) to (4.37) are modulation equations that relates the converter state variables with the control and input variables. The output equation described in equation (4.6) can be expressed in terms of the above variables as

$$V_O=\left(\frac{2}{\pi}I_P+i_o\right)r_o+V_{Cf}\frac{r_o}{r_{Cf}}, \tag{4.38}$$

where I_P represents the $|i_m|=\sqrt{I_S^2+I_C^2}$ and $r_o=\frac{r_{Cf}R_L}{r_{Cf}+R_L}$.

4.4 Steady-state Analysis

Using the quantities I_S, I_C, V_S, V_C, and V_{Cf}, the steady-state model of the series resonant converter can be derived. Under steady-state conditions, the output DC-bias current $i_o = I_O$ will be equal to 0. Also, the time varying quantities dI_C/dt, dI_S/dt, dV_C/dt, dV_S/dt and dV_{Cf}/dt are zero since they do not change with time under steady-state. Equations (4.33) to (4.37) can be re-written as

$$L\left(\frac{dI_C}{dt}\right)=-LI_S\omega_s-r_SI_C-V_C-\frac{4V_{Cf}}{\pi I_P}I_C, \tag{4.39}$$

$$L\left(\frac{dI_S}{dt}\right)=\frac{2V_I}{\pi}\sin\left(\frac{\pi D}{2}\right)+LI_C\omega_s-r_SI_S-V_S-\frac{4V_{Cf}}{\pi I_P}I_S, \tag{4.40}$$

$$C\left(\frac{dV_C}{dt}\right)=I_C-C\omega_sV_S, \tag{4.41}$$

$$C\left(\frac{dV_S}{dt}\right)=I_S+C\omega_sV_C, \tag{4.42}$$

$$C_f\left(\frac{dV_{Cf}}{dt}\right)=\frac{2I_P}{\pi}-\frac{V_O}{R_L}. \tag{4.43}$$

Applying the steady-state substitutions, we obtain

$$-LI_S\omega_s-r_SI_C-V_C-\frac{4V_{Cf}I_C}{\pi I_P}=0, \tag{4.44}$$

$$\frac{2V_I}{\pi}\sin\left(\frac{\pi D}{2}\right) + LI_C\omega_s - r_S I_S - V_S - \frac{4V_{Cf}I_S}{\pi I_P} = 0, \tag{4.45}$$

$$I_C - C\omega_s V_S = 0, \tag{4.46}$$

$$I_S + C\omega_s V_C = 0, \tag{4.47}$$

$$\frac{2I_P}{\pi} - \frac{V_O}{R_L} = 0. \tag{4.48}$$

Now the new steady-state variables I_C, I_C, V_C, V_S, and V_{Cf} can be derived in terms of the control and input variables. Consider (4.48).

$$\frac{V_O}{R_L} = \frac{2I_P}{\pi}.$$

The voltage drop across r_{Cf} is assumed to be very small when compared to V_{Cf}, hence

$$V_{Cf} = V_O = \frac{2I_P R_L}{\pi}. \tag{4.49}$$

Equations (4.46) and (4.47) become

$$I_C = \omega_s C V_S, \tag{4.50}$$

$$I_S = -\omega_s C V_C. \tag{4.51}$$

Substituting (4.49) and (4.50) in (4.44),

$$LI_S\omega_s = -r_S I_C - \left(-\frac{I_S}{\omega_s C}\right) - \frac{8R_L}{\pi^2}I_C,$$

$$LI_S\omega_s = -r_S I_C + \left(\frac{I_S}{\omega_s C}\right) - \frac{8R_L}{\pi^2}I_C,$$

$$I_S\left(L\omega_s - \frac{1}{C\omega_s}\right) = -I_C\left[r_S + \frac{8R_L}{\pi^2}\right].$$

Let

$$\alpha = \left(L\omega_s - \frac{1}{C\omega_s}\right), \tag{4.52}$$

$$= L\omega_o\left(\frac{\omega_s}{\omega_o} - \frac{\omega_o}{\omega_s}\right) = \frac{L\omega_o R}{R}\left(\frac{\omega_s}{\omega_o} - \frac{\omega_o}{\omega_s}\right)$$

$$= RQ_L \left(\frac{\omega_s}{\omega_o} - \frac{\omega_o}{\omega_s} \right), \tag{4.53}$$

where $\omega_o = \frac{1}{\sqrt{LC}}$, $Q_L = \frac{\omega_o L}{R}$, and $R = R_e + r_S$. Let and

$$\beta = \left(r_S + \frac{8R_L}{\pi^2} \right), \tag{4.54}$$

then,

$$I_S \alpha = -I_C \beta,$$

$$I_S = -\frac{I_C}{\alpha} \beta.$$

Substituting (4.49) and (4.51) in (4.45)

$$-LI_C\omega_s = \frac{2V_I}{\pi} \sin\left(\frac{\pi D}{2}\right) - r_S I_S - \left(\frac{I_C}{\omega_s C}\right) - \frac{8I_S R_L}{\pi^2 I_P},$$

$$I_C \left(-\omega_s L + \frac{1}{\omega_s C} \right) = \frac{2V_I}{\pi} \sin\left(\frac{\pi D}{2}\right) - I_S \left(r_s + \frac{8R_L}{\pi^2} \right),$$

i.e.,

$$I_C(-\alpha) = \frac{2V_I}{\pi} \sin\left(\frac{\pi D}{2}\right) - I_S \beta.$$

Substituting for I_S in above equation,

$$I_C(-\alpha) = \frac{2V_I}{\pi} \sin\left(\frac{\pi D}{2}\right) - \left(-\frac{I_C}{\alpha} \beta \right) \beta,$$

$$I_C(-\alpha) = \frac{2V_I}{\pi} \sin\left(\frac{\pi D}{2}\right) - \left(\frac{I_C \beta^2}{\alpha} \right),$$

$$I_C \left(-\alpha - \frac{\beta^2}{\alpha} \right) = \frac{2V_I}{\pi} \sin\left(\frac{\pi D}{2}\right),$$

$$I_C = -V_e \frac{\alpha}{\alpha^2 + \beta^2}, \tag{4.55}$$

where

$$V_e = \frac{2V_I}{\pi} \sin\left(\frac{\pi D}{2}\right). \tag{4.56}$$

Substituting I_C in I_S

$$I_S = -\left(\frac{-V_e \alpha}{\alpha^2 + \beta^2} \right) \frac{\beta}{\alpha},$$

$$I_S = V_e \frac{\beta}{\alpha^2 + \beta^2}. \tag{4.57}$$

$$I_P = \sqrt{\left(\frac{-V_e\alpha}{\alpha^2+\beta^2}\right)^2 + \left(\frac{V_e\beta}{\alpha^2+\beta^2}\right)^2},$$

$$I_P = \frac{V_e}{\alpha^2+\beta^2}\sqrt{\alpha^2+\beta^2},$$

$$I_P = \frac{V_e}{\alpha^2+\beta^2}. \tag{4.58}$$

From equations (4.50) and (4.51)

$$V_C = -V_e \frac{\beta}{\omega_s C\left(\alpha^2+\beta^2\right)}, \tag{4.59}$$

$$V_S = -V_e \frac{\alpha}{\omega_s C\left(\alpha^2+\beta^2\right)}. \tag{4.60}$$

The voltage across the filter capacitor V_{Cf} can be expressed as

$$V_{Cf} = \frac{2V_e R_L}{\pi(\alpha^2+\beta^2)}. \tag{4.61}$$

Substituting equation (4.58) in the output equation given in (4.38), we obtain

$$V_O = \frac{2}{\pi} I_P r_o + V_{Cf}\frac{r_o}{r_{Cf}}. \tag{4.62}$$

4.5 Derivation of Small-signal Model

With the steady-state analysis, the converter behaviour at various operating points can be understood. When these converters are connected to the supply, they undergo abrupt variations in the input voltage and load relocating the operating point. Thus, it is essential to determine the effect on the converter due to these variations. Control schemes that include duty-cycle control and frequency control are required in order to maintain constant output parameters. Hence, a small-signal model is derived in order to understand the converter response for these small-signal changes. In order to derive the small-signal model of a DC-DC converter, it is essential to linearize the switching components and express it as a linear model. The derived state equations

are perturbed and linearized about their operating point to perform small-signal analysis. The state variable vector and control and input variables vector can be expressed as

$$\vec{X} = \begin{bmatrix} I_C \\ I_S \\ V_C \\ V_S \\ V_{Cf} \end{bmatrix}, \tag{4.63}$$

and

$$\vec{U} = \begin{bmatrix} V_I \\ D \\ \omega_s \\ I_O \end{bmatrix}. \tag{4.64}$$

The steady-state quantities represented in $\vec{X}$ and $\vec{U}$ can be replaced by slowly varying, time dependent, large-signal quantities. Consider the series resonant converter being subjected to a low frequency perturbation about the DC value. The large-signal model can be considered as a low-frequency perturbation about the operating point, i.e. a low-frequency excitation superimposed on the DC value of the variables. Such an excitation appears in all the waveforms of the converter resulting in large-signal model. A large-signal model consists of

- a DC component
- low-frequency component of frequency $f = \omega/2\pi \leq f_s/2$ along with its harmonics
- high-frequency component of switching frequency f_s and its harmonics.

Thus $\vec{X}$ and $\vec{U}$ can now be expressed as vectors consisting of the large-signal quantities given as follows

$$\vec{x} = \begin{bmatrix} i_C \\ i_S \\ v_C \\ v_S \\ v_{Cf} \end{bmatrix}, \quad \vec{u} = \begin{bmatrix} v_I \\ d_T \\ \omega_S \\ i_O \end{bmatrix} \tag{4.65}$$

Detailed description about large-signal modeling of DC-DC converters is provided in [20]. So, if the steady-state variables V_I and D are perturbed at a low frequency $f \leq f_s/2$, then all other quantities will fluctuate about this level at a low frequency resulting in the large-signal model which can be represented as

$$i_C = I_C + \hat{i_c}, \tag{4.66}$$

$$i_S = I_S + \hat{i_s}, \tag{4.67}$$

$$v_C = V_C + \hat{v_c}, \tag{4.68}$$

$$v_S = V_S + \hat{v_s}. \tag{4.69}$$

The input and control variables can be expressed as

$$v_I = V_I + \hat{v_i}, \tag{4.70}$$

$$d_T = D + \hat{d}, \tag{4.71}$$

$$\omega_S = \omega_s + \hat{\omega_s}, \tag{4.72}$$

$$i_O = I_O + \hat{i_o}, \tag{4.73}$$

$$v_O = V_O + \hat{v_o}. \tag{4.74}$$

Based on our analysis under steady-state, the DC bias current I_O will be equal to zero and only its small-signal quantity $\hat{i_o}$ is considered. Representing the variables in (4.39) to (4.43) and 4.38 in terms of large-signal quantities, we obtain

$$L\left(\frac{di_C}{dt}\right) = -Li_S\omega_S - r_S i_C - v_C - \frac{4v_{Cf}}{\pi I_P} i_C, \tag{4.75}$$

$$L\left(\frac{di_S}{dt}\right) = \frac{2v_I}{\pi}\sin\left(\frac{\pi d_T}{2}\right) + Li_C\omega_S - r_S i_S - v_S - \frac{4v_{Cf} i_S}{\pi I_P}, \tag{4.76}$$

$$C\left(\frac{dv_C}{dt}\right) = i_C - C\omega_S v_S, \tag{4.77}$$

$$C\left(\frac{dv_S}{dt}\right) = i_S + \omega_S v_C, \tag{4.78}$$

$$C_f \frac{dv_{Cf}}{dt} = \frac{2I_P}{\pi} - \frac{v_O}{R_L} + i_O. \tag{4.79}$$

$$v_O = \left(\frac{2}{\pi} I_P + i_O\right) r_o + v_{Cf} \frac{r_o}{r_{Cf}} \tag{4.80}$$

The model presented in the above set of differential equations is highly non-linear. It is essential to obtain the linear model of the converter in order to understand the system behaviour for variation in input parameters. Hence, linearization of the large-signal model is performed by expanding the non-linear differential equations about the operating point and then, ignoring the higher order terms [20]. Re-writing the above equations,

$$L\left[\frac{d(I_C + \hat{i_c})}{dt}\right] = -L(I_S + \hat{i_s})(\omega_s + \hat{\omega_s}) - r_S(I_C + \hat{i_c}) - (V_C + \hat{v_c}) - \frac{4\hat{v_{Cf}}}{\pi I_P}(I_C + \hat{i_c}), \tag{4.81}$$

$$L\left[\frac{d(I_S + \hat{i_s})}{dt}\right] = \frac{2(V_I + \hat{v_i})}{\pi} \sin\left[\frac{\pi(D + \hat{d})}{2}\right] + L(I_C + \hat{i_c})(\omega_s + \hat{\omega_s}) - r_S(I_S + \hat{i_s}) - (V_S + \hat{v_s}) - \frac{4\hat{v_{Cf}}(I_S + \hat{i_s})}{\pi I_P}, \tag{4.82}$$

$$C\left[\frac{d(V_C + \hat{v_c})}{dt}\right] = (I_C + \hat{i_c}) - C(\omega_s + \hat{\omega_s})(V_S + \hat{v_s}), \tag{4.83}$$

$$C\left[\frac{d(V_S + \hat{v_s})}{dt}\right] = (I_S + \hat{i_s}) + C(\omega_s + \hat{\omega_s})(V_C + \hat{v_c}), \tag{4.84}$$

$$C_f \frac{d\hat{v_{Cf}}}{dt} = \frac{2I_P}{\pi} - \frac{V_O + \hat{v_o}}{R_L} + \hat{i_o} \tag{4.85}$$

and

$$V_O + \hat{v_o} = \frac{2}{\pi} I_P r_o + (I_O + \hat{i_o}) r_o + \hat{v_{Cf}} \frac{r_o}{r_{Cf}}. \tag{4.86}$$

Equations (4.81) to (4.86) can be further represented as,

$$L\left[\frac{d(I_C + \hat{i_c})}{dt}\right] = -L[I_S\omega_s + I_S\hat{\omega_s} + \hat{i_s}\omega_s + \hat{i_s}\hat{\omega_s}] - r_s I_C - r_s\hat{i_c} - V_C - \hat{v_c} - \frac{4\hat{v_{Cf}}\hat{i_c}}{I_P} - \frac{4\hat{v_{Cf}} I_C}{I_P},$$

$$L\left[\frac{d(I_S+\hat{i_s})}{dt}\right]=\frac{2V_I}{\pi}\sin\left[\frac{\pi(D+\hat{d})}{2}\right]+\frac{2\hat{v_i}}{\pi}\sin\left[\frac{\pi(D+\hat{d})}{2}\right]+$$

$$Ł(I_C\omega_s+I_C\hat{\omega_s}+\hat{i_c}\omega_s+\hat{i_c}\hat{\omega_s})-r_SI_S-r_S\hat{i_s}-V_S-\hat{v_s}-\frac{4\hat{v_{Cf}}\hat{i_s}}{I_P}-\frac{4\hat{v_{Cf}}I_S}{I_P},$$

$$C\left[\frac{d(V_C+\hat{v_c})}{dt}\right]=(I_C+\hat{i_c})-C(\omega_sV_S+\omega_s\hat{v_s}+\hat{\omega_s}V_S+\hat{\omega_s}\hat{v_s}),$$

$$C\left[\frac{d(V_S+\hat{v_s})}{dt}\right]=(I_S+\hat{i_s})+C(\omega_sV_C+\omega_s\hat{v_c}+\hat{\omega_s}V_C+\hat{\omega_s}\hat{v_c}),$$

$$C_f\frac{d\hat{v_{Cf}}}{dt}=\frac{\hat{i_s}I_P}{\pi I_S}+\frac{\hat{i_c}I_P}{\pi I_C}-\frac{V_O+\hat{v_o}}{R_L}+\hat{i_o}.$$

$$V_O+\hat{v_o}=\frac{2}{\pi}I_Pr_o+I_Or_o+\hat{i_o}r_o+\hat{v_{Cf}}\frac{r_o}{r_{Cf}}. \tag{4.87}$$

The above set of equations represent the large-signal model which is highly non-linear due to the presence of small-signal components. Linearization allows the assumption that the amplitudes of the ac low-frequency components are significantly lower than that of the corresponding DC components. Hence,

$$\hat{i_s}\hat{\omega_s}\ll\hat{i_s}\omega_s,$$

$$\hat{i_c}\hat{\omega_s}\ll\hat{i_c}\omega_s,$$

$$\hat{v_s}\hat{\omega_s}\ll\hat{v_s}\omega_s,$$

$$\hat{v_c}\hat{\omega_s}\ll\hat{v_c}\omega_s,$$

$$\hat{v_{Cf}}\hat{i_c}\ll\hat{v_{Cf}}I_C,$$

$$\hat{v_{Cf}}\hat{i_s}\ll\hat{v_{Cf}}I_S. \tag{4.88}$$

Based on the the assumptions provided in (4.88), the large-signal model consisting of non-linear differential equations is linearized and expressed as a set of linear differential equations as follows.

$$L\left[\frac{d(I_C+\hat{i_c})}{dt}\right] = -L(I_S\omega_s + I_S\hat{\omega_s} + \hat{i_s}\omega_s) - r_sI_C - r_s\hat{i_c} - V_C - \hat{v_c} - \frac{4\hat{v_{Cf}}I_C}{I_P}, \quad (4.89)$$

$$L\left[\frac{d(I_S+\hat{i_s})}{dt}\right] = \frac{2}{\pi}\sin\left(\frac{\pi D}{2}\right)\hat{v_i} + 2V_I\cos\left(\frac{\pi D}{2}\right)\hat{d} + L(I_C\omega_s + I_C\hat{\omega_s} + \hat{i_c}\omega_s) -$$
$$r_SI_S - r_S\hat{i_s} - V_S - \hat{v_s} - \frac{4\hat{v_{Cf}}I_S}{I_P}, \quad (4.90)$$

$$C\left[\frac{d(V_C+\hat{v_c})}{dt}\right] = (I_C+\hat{i_c}) - C(\omega_sV_S + \omega_s\hat{v_s} + \hat{\omega_s}V_S), \quad (4.91)$$

$$C\left[\frac{d(V_S+\hat{v_s})}{dt}\right] = (I_S+\hat{i_s}) + C(\omega_sV_C + \omega_s\hat{v_c} + \hat{\omega_s}V_C), \quad (4.92)$$

$$C_f\frac{d\hat{v_{Cf}}}{dt} = \frac{\hat{i_s}I_P}{\pi I_S} + \frac{\hat{i_c}I_P}{\pi I_C} - \frac{V_O+\hat{v_o}}{R_L} + \hat{i_o}. \quad (4.93)$$

The principle of superposition can be applied to linear models, where the DC and ac small-signal terms can be seperated into two different set of equations. Extracting the ac components from the equations (4.89) to (4.93) and 4.86, we obtain

$$L\left(\frac{d\hat{i_c}}{dt}\right) = -L(I_S\hat{\omega_s} + \hat{i_s}\omega_s) - r_s\hat{i_c} - \hat{v_c} - \frac{4\hat{v_{Cf}}I_C}{I_P}, \quad (4.94)$$

$$L\left(\frac{d\hat{i_s}}{dt}\right) = \frac{2}{\pi}\sin\left(\frac{\pi D}{2}\right)\hat{v_i} + 2V_I\cos\left(\frac{\pi D}{2}\right)\hat{d} + L(I_C\hat{\omega_s} + \hat{i_c}\omega_s)$$
$$-r_S\hat{i_s} - \hat{v_s} - \frac{4\hat{v_{Cf}}I_S}{I_P}, \quad (4.95)$$

$$C\left[\frac{d\hat{v_c}}{dt}\right] = \hat{i_c} - C(\omega_s\hat{v_s} + \hat{\omega_s}V_S), \quad (4.96)$$

$$C\left[\frac{d\hat{v_s}}{dt}\right] = \hat{i_s} + C(\omega_s \hat{v_c} + \hat{\omega_s} V_C), \tag{4.97}$$

The small-signal variable $\hat{v_o}$ can be considered to be equal to $\hat{v_{Cf}}$ in further analysis.

$$C_f \frac{d\hat{v_{Cf}}}{dt} = \frac{\hat{i_s} I_P}{\pi I_S} + \frac{\hat{i_c} I_P}{\pi I_C} - \frac{\hat{v_{Cf}}}{R_L} + \hat{i_o}, \tag{4.98}$$

and the output voltage is

$$\hat{v_o} = \frac{\hat{i_s} I_P}{\pi I_S} + \frac{\hat{i_c} I_P}{\pi I_C} + \hat{i_o} r_o + \hat{v_{Cf}} \frac{r_o}{r_{Cf}}. \tag{4.99}$$

Equations (4.94) to (4.98) represent the small-signal model of the series resonant converter derived using the extended describing function approximations. Expressing these equations in standard linear differential equation form, we obtain

$$\frac{d\hat{i_c}}{dt} = \frac{1}{L}\left[-L(I_S \hat{\omega_s} + \hat{i_s}\omega_s) - r_s \hat{i_c} - \hat{v_c} - \frac{4\hat{v_{Cf}} I_C}{I_P}\right], \tag{4.100}$$

$$\frac{d\hat{i_s}}{dt} = \frac{1}{L}\left[\frac{2}{\pi}\sin\left(\frac{\pi D}{2}\right)\hat{v_i} + 2V_I \cos\left(\frac{\pi D}{2}\right)\hat{d} + L(I_C \hat{\omega_s} + \hat{i_c}\omega_s) - r_S \hat{i_s} - \hat{v_s} - \frac{4\hat{v_{Cf}} I_S}{I_P}\right], \tag{4.101}$$

$$\frac{d\hat{v_c}}{dt} = \frac{1}{C}\left[\hat{i_c} - C(\omega_s \hat{v_s} + \hat{\omega_s} V_S)\right], \tag{4.102}$$

$$\frac{d\hat{v_s}}{dt} = \frac{1}{C}\left[\hat{i_s} + C(\omega_s \hat{v_c} + \hat{\omega_s} V_C)\right], \tag{4.103}$$

$$\frac{d\hat{v_{Cf}}}{dt} = \frac{1}{C_f}\left(\frac{\hat{i_s} I_P}{\pi I_S} + \frac{\hat{i_c} I_P}{\pi I_C} - \frac{\hat{v_{Cf}}}{R_L} + \hat{i_o}\right). \tag{4.104}$$

and the output equation can be expressed as

$$\hat{v_o} = \frac{\hat{i_s} I_P}{\pi I_S} + \frac{\hat{i_c} I_P}{\pi I_C} + \hat{i_o} r_o + \hat{v_{Cf}} \frac{r_o}{r_{Cf}}. \tag{4.105}$$

The above set of differential equations can be expressed in terms of transfer matrix representation. The general form of transfer matrix is expressed as

$$\frac{d\hat{x}}{dt} = A\hat{x} + B\hat{u},$$

$$\hat{y} = C\hat{x} + D\hat{u}. \tag{4.106}$$

where

$$\hat{x} = \begin{bmatrix} \hat{i_c} \\ \hat{i_s} \\ \hat{v_c} \\ \hat{v_s} \\ \hat{v_{Cf}} \end{bmatrix}, \quad \hat{u} = \begin{bmatrix} \hat{v_i} \\ \hat{d} \\ \hat{\omega_s} \\ \hat{i_o} \end{bmatrix}. \tag{4.107}$$

Therefore,

$$\begin{bmatrix} \frac{d\hat{i_c}}{dt} \\ \frac{d\hat{i_s}}{dt} \\ \frac{d\hat{v_c}}{dt} \\ \frac{d\hat{v_s}}{dt} \\ \frac{d\hat{v_{Cf}}}{dt} \end{bmatrix} = \begin{bmatrix} \frac{-r_s}{L} & \frac{-\omega_s L}{L} & \frac{-1}{L} & 0 & -\frac{4I_C}{\pi I_P L} \\ \frac{\omega_s L}{L} & \frac{-r_s}{L} & 0 & \frac{-1}{L} & -\frac{4I_S}{\pi I_P L} \\ \frac{1}{C} & 0 & 0 & \frac{-C\omega_s}{C} & 0 \\ 0 & \frac{1}{C} & \frac{C\omega_s}{C} & 0 & 0 \\ \frac{I_P}{\pi I_C} & \frac{I_P}{\pi I_S} & 0 & 0 & \frac{-1}{R_L C_f} \end{bmatrix} \begin{bmatrix} \hat{i_c} \\ \hat{i_s} \\ \hat{v_c} \\ \hat{v_s} \\ \hat{v_{Cf}} \end{bmatrix}$$
$$+ \begin{bmatrix} 0 & 0 & \frac{-LI_S}{L} & 0 \\ \frac{2}{\pi}\sin\left(\frac{\pi D}{2}\right) & 2V_I\cos\left(\frac{\pi D}{2}\right) & \frac{LI_C}{L} & 0 \\ 0 & 0 & \frac{-CV_S}{C} & 0 \\ 0 & 0 & \frac{-CV_C}{C} & 0 \\ 0 & 0 & 0 & \frac{1}{C_f} \end{bmatrix} \begin{bmatrix} \hat{v_i} \\ \hat{d} \\ \hat{\omega_s} \\ \hat{i_o} \end{bmatrix}. \tag{4.108}$$

The output matrix $[\hat{y}]$ is given as

$$[\hat{v_o}] = \begin{bmatrix} \frac{I_P r_o}{\pi I_C} & \frac{I_P r_o}{\pi I_S} & 0 & 0 & r_o \end{bmatrix} \begin{bmatrix} \hat{i_c} \\ \hat{i_s} \\ \hat{v_c} \\ \hat{v_s} \\ \hat{v_{Cf}} \end{bmatrix} + \begin{bmatrix} 0 & 0 & 0 & \frac{r_o}{r_{Cf}} \end{bmatrix} \begin{bmatrix} \hat{v_i} \\ \hat{d} \\ \hat{\omega_s} \\ \hat{i_o} \end{bmatrix}. \tag{4.109}$$

The matrices $[A], [B], [C]$, and $[D]$ can be further represented as

$$[A] = \begin{bmatrix} \frac{-r_s}{L} & \frac{-Z_1}{L} & \frac{-1}{L} & 0 & -\frac{4I_C}{\pi I_P L} \\ \frac{Z_1}{L} & \frac{-r_s}{L} & 0 & \frac{-1}{L} & -\frac{4I_S}{\pi I_P L} \\ \frac{1}{C} & 0 & 0 & \frac{-1}{Z_2 C} & 0 \\ 0 & \frac{1}{C} & \frac{1}{Z_2 C} & 0 & 0 \\ K_C & K_S & 0 & 0 & \frac{-1}{R_L C_f} \end{bmatrix}, \tag{4.110}$$

$$[B] = \begin{bmatrix} 0 & 0 & \frac{-G_S}{L} & 0 \\ \frac{2}{\pi}\sin\left(\frac{\pi D}{2}\right) & 2V_I\cos\left(\frac{\pi D}{2}\right) & \frac{G_C}{L} & 0 \\ 0 & 0 & \frac{-J_S}{C} & 0 \\ 0 & 0 & \frac{-J_C}{C} & 0 \\ 0 & 0 & 0 & \frac{1}{C_f} \end{bmatrix} \begin{bmatrix} \hat{v_i} \\ \hat{d} \\ \hat{\omega_s} \\ \hat{i_o} \end{bmatrix}, \tag{4.111}$$

$$[C] = \begin{bmatrix} K_C r_o & K_S r_o & 0 & 0 & r_o \end{bmatrix}, \tag{4.112}$$

and

$$[D] = \begin{bmatrix} 0 & 0 & 0 & \frac{r_o}{r_{Cf}} \end{bmatrix} \tag{4.113}$$

where

$$\begin{aligned} Z_1 &= \omega_s L, \quad Z_2 = \frac{1}{\omega_s C}, \\ K_C &= \frac{I_P}{\pi I_C}, \quad K_S = \frac{I_P}{\pi I_S}, \\ G_S &= LI_S, \quad G_C = LI_C, \\ J_S &= CV_S, \quad J_C = CV_C, \\ r_o &= \frac{r_{Cf} R_L}{R_{Cf} + R_L}. \end{aligned} \tag{4.114}$$

The matrix A gives a relation between the derivatives of the states and the state variables. Matrix B is the input matrix. It provides a relation between the derivative of the state variables with the inputs and control variables. The matrix C relates the states with the output of the converter, and matrix D is known as the direct transmission matrix that represent those elements which transmit input directly to the output of the system. The equivalent circuit model of the series resonant converter

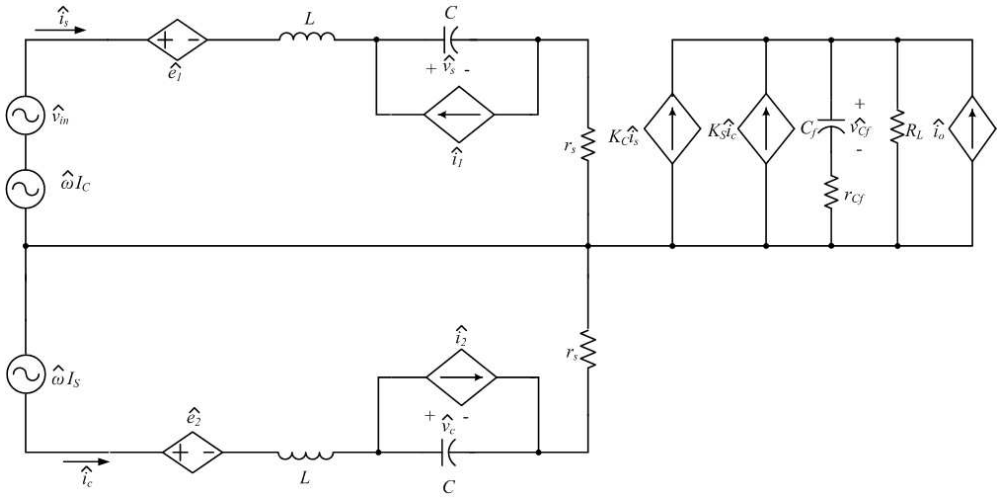

Figure 4.3: Equivalent small-signal model of series resonant converter.

is shown in Figure 4.3. The circuit model can be represented based on the differential equations from the transfer matrix. The two loops represent the co-sinusoidal and sinusoidal components of the small-signal state equations. The upper loop is driven by the current $\hat{i_s}$ and represent the sinusoidal component of state equations. Similarly, the bottom loops represents the loop due to the co-sinusoidal component $\hat{i_c}$. Several quantities are lumped for the sake of simplicity and are expressed as follows.

$$\hat{v_{in}} = \frac{4}{\pi}\sin\left(\frac{\pi D}{2}\right)\hat{v_i} + V_I\cos\left(\frac{\pi D}{2}\right)\hat{d},$$

$$\hat{e_1} = -Z_1\hat{i_c} - \frac{4I_C}{\pi I_P}\hat{v_{Cf}},$$

$$\hat{e_2} = Z_1\hat{i_s} - \frac{4I_S}{\pi I_P}\hat{v_{Cf}},$$

$$\hat{i_1} = -Z_2\hat{v_c} - J_S\hat{\omega_s},$$

$$\hat{i_2} = Z_2\hat{v_s} + J_C\hat{\omega_s}. \tag{4.115}$$

5 Design of Series Resonant Converter

In this chapter, the steady-state voltage and currents across various components are evaluated. With the help of frequency-domain analysis, behaviour of the converter at various operating points is understood. From the knowledge of small-signal modeling provided in Chapter 4, steady-state quantities are evaluated and hence, by providing a small-signal disturbance at the input and control variables, various transfer functions are derived. With these data in hand, it is possible to design a SRC for a practical application as follows.

For the following specifications, design a non-isolated SRC with a bridge rectifier. Given, $V_I = 180$ V, $V_O = 75$ V, $R_L = 200\ \Omega$ to 1 kΩ. The esr of the components are $r_L = 25$ mΩ and $r_C = 25$ mΩ, and $r_{Cf} = 25$ mΩ. The diode parameters are $R_F = 0.1\ \Omega$ and $V_F = 0.7$ V. The total inverter efficiency is assumed to be unity. The resonant frequency is set at $f_o = 102$ kHz and the switching frequency is $f = 110$ kHz.

5.1 Solution

5.1.1 Design of Converter Components

The converter is designed for a full load resistance of $R_{Lmin} = 200\ \Omega$. The maximum output current I_{Omax} is expressed as

$$I_{Omin} = \frac{V_O}{R_{Lmax}} = \frac{75}{1000} = 0.075 \text{ A}, \tag{5.1}$$

$$I_{Omax} = \frac{V_O}{R_{Lmin}} = \frac{75}{200} = 0.375 \text{ A}. \tag{5.2}$$

The maximum output power P_{Omax} is

$$P_{Omax} = V_O \times I_{Omax} = 75 \times 0.375 = 28.125 \text{ W} \tag{5.3}$$

and the minimum output power P_{Omin} is

$$P_{Omin} = V_O \times I_{Omin} = 75 \times 0.075 = 5.625 \text{ W}. \tag{5.4}$$

The efficiency of the bridge rectifier η_R is given by [15]

$$\eta_R = \frac{1}{\left[1 + \frac{2V_F}{V_O} + \frac{\pi^2 R_F}{4R_L} + \frac{r_{Cf}}{R_L}\left(\frac{\pi^2}{8} - 1\right)\right]}$$

$$= \frac{1}{\left[1 + \frac{2\times 0.7}{75} + \frac{\pi^2\times 0.1}{4\times 200} + \frac{0.025}{200}\left(\frac{\pi^2}{8} - 1\right)\right]} = 96.28\% \tag{5.5}$$

The voltage gain M_{VR} of the bridge rectifier is expressed as

$$M_{VR} = \frac{\pi}{2\sqrt{2}\left[1 + \frac{2V_F}{V_o} + \frac{\pi^2 R_F}{4R_L} + \frac{r_{Cf}}{R_L}\left(\frac{\pi^2}{8} - 1\right)\right]} = \frac{\pi\eta_R}{2\sqrt{2}}$$

$$= \frac{\pi \times 0.9628}{2\sqrt{2}} = 1.0685 \tag{5.5}$$

The voltage transfer function M_{Vr} of the resonant circuit is given by

$$M_{Vr} = \frac{M_V}{M_{Vs} \times M_{VR}}, \tag{5.5}$$

where $M_V = V_O/V_I = 75/180 = 0.4166$ and $M_{Vs} = \sqrt{2}/\pi = 0.45$, then,

$$M_{Vr} = \frac{0.4166}{0.45 \times 1.0685} = 0.8664. \tag{5.5}$$

In order to determine the value of resonant inductance L and capacitance C, the quality factor Q_L needs to be determined. The switching frequency f is normalized with respect to the resonant frequency, hence $f/f_o = 110/102 = 1.07$. Equation (2.27) can be modified to include the efficiency of the inverter η_I. The expression for M_{Vr} is given by

$$|M_{Vr}| = \frac{\eta_I}{\sqrt{1 + {Q_L}^2\left(\frac{\omega}{\omega_o} - \frac{\omega_o}{\omega}\right)^2}},$$

$$Q_L^2\left(\frac{\omega}{\omega_o} - \frac{\omega_o}{\omega}\right)^2 = \frac{\eta_I^2}{M_{Vr}^2} - 1$$

$$Q_L = \sqrt{\frac{\eta_I^2 - M_{Vr}^2}{M_{Vr}^2\left(\frac{\omega}{\omega_o} - \frac{\omega_o}{\omega}\right)^2}} = \frac{\sqrt{\frac{\eta_I^2}{M_{Vr}^2} - 1}}{\left(\frac{\omega}{\omega_o} - \frac{\omega_o}{\omega}\right)} \tag{5.3}$$

$$= \frac{\sqrt{\frac{1}{0.8664^2} - 1}}{\left(1.07 - \frac{1}{1.07}\right)} = 4.256 \tag{5.3}$$

From equation (2.14), $R = R_e + r$. For the bridge rectifer the effective input resistance is given by

$$R_e = \frac{8R_L}{\pi^2}\left[1 + \frac{2V_F}{V_O} + \frac{\pi^2 R_F}{4R_L} + \frac{r_{Cf}}{R_L}\left(\frac{\pi^2}{8} - 1\right)\right] = \frac{8R_L}{\pi^2\eta_R} \tag{5.3}$$

$$= \frac{8 \times 200}{\pi^2 \times 0.9628} = 168.54\ \Omega. \tag{5.3}$$

The sum of the equivalent series resistances is $r = r_L + r_C = 0.025 + 0.025 = 0.05\ \Omega$. The overall resistance of the converter is given by

$$R = \frac{R_e + r}{\eta_I} = \frac{168.54 + 0.05}{1} = 168.59\ \Omega \tag{5.3}$$

From (2.14), the component values can be obtained as follows. The value of resonant inductance L is

$$L = \frac{Q_L R}{\omega_o} = \frac{4.256 \times 168.59}{2 \times \pi \times 102 \times 10^3} = 1.120\ \text{mH}. \tag{5.3}$$

The value of the resonant capacitance C is

$$C = \frac{1}{\omega_o Q_L R} = \frac{1}{2 \times \pi \times 102 \times 10^3 \times 1.867 \times 183.25} = 2.17\ \text{nF}. \tag{5.3}$$

Using equation (2.13),

$$Z_O = \sqrt{\frac{L}{C}} = \sqrt{\frac{1.120 \times 10^{-3}}{2.17 \times 10^{-9}}} = 718.42\ \Omega. \tag{5.3}$$

The maximum ripple voltage across the filter capacitor is [15]

$$V_r = 0.002 V_O = 0.002 \times 75 = 0.15\ \text{V}. \tag{5.3}$$

The voltage across the esr is expressed as

$$V_{rESR} = \frac{\pi}{2} r_{Cf} I_{Omax} = \frac{\pi}{2} \times 0.025 \times 0.375 = 0.0147\ \text{V}. \tag{5.3}$$

The voltage across the filter capacitor is

$$V_{Cf} = V_r - V_{rESR} = 0.15 - 0.0147 = 0.1353\ \text{V}. \tag{5.3}$$

The minimum value of the filter capacitance is expressed as [15]

$$C_f = \frac{0.105 I_{Omin}}{f V_{Cf}} = \frac{0.105 \times 0.075}{110 \times 10^3 \times 0.1353} = 529 \text{ nF}. \tag{5.3}$$

The maximum stress across the switches is

$$V_{SM} = V_I = 180 \text{ V}. \tag{5.3}$$

From equations (2.33) and (2.34), the peak voltage stress across the resonant inductor and capacitor is

$$V_{Lm} = V_{Cm} = \frac{2 V_I Q_L}{\pi} = \frac{2 \times 180 \times 4.256}{3.14} \approx 488 \text{ V}. \tag{5.3}$$

The peak value of current I_{DM} and voltage V_{DM} across the diodes is

$$I_{DM} = \frac{\pi I_{O_{max}}}{2} = \frac{3.14 \times 0.375}{2} = 0.58875 \text{ A}, \tag{5.3}$$

$$V_{DM} = V_O = 75 \text{ V}. \tag{5.3}$$

The maximum value of output current is is given by

$$I_O = \frac{2 I_{DM}}{\pi} = \frac{2 \times 0.58875}{\pi} = 0.375 \text{ A}. \tag{5.3}$$

The overall converter efficiency can be calculated as

$$\eta = \eta_I \eta_R = 1 \times 0.9628 = 0.9628. \tag{5.3}$$

The DC input power at full load is given by

$$P_{Imax} = \frac{P_{Omax}}{\eta} = \frac{28.125}{0.9628} = 29.21 \text{ W}. \tag{5.3}$$

From the calculated value of input power P_{Imax}, the peak value of switch current is

$$I_{SM_{max}} = \sqrt{\frac{2 P_{Imax} \eta_I}{R_e}} = \sqrt{\frac{2 \times 29.21 \times 1}{168.59}} = 0.588 \text{ A}. \tag{5.3}$$

5.1.2 Derivation of Small-signal Transfer Matrix

The steady-state variables are derived in Chapter 4 using the first harmonic approximation approach. Using equations (4.52) to (4.62), it is possible to evaluate the the converter response for different frequencies. For simplicity, the switching frequency is expressed as f_s and total esr r is expressed as r_s. The value of duty-ratio $D = 1$. The steady-state parameters are evaluated as follows.

$$\alpha = \left(L\omega_s - \frac{1}{C\omega_s}\right) = RQ_L\left(\frac{\omega_s}{\omega_o} - \frac{\omega_o}{\omega_s}\right),$$
$$= 168.59 \times 4.256 \times \left(1.07 - \frac{1}{1.07}\right) = 97.1668\ \Omega, \tag{5.2}$$
$$\beta = \left(r_s + \frac{8R}{\pi^2}\right)$$
$$= \left(0.05 + \frac{8 \times 168.59}{\pi^2}\right) = 162.1639\ \Omega. \tag{5.1}$$
$$V_e = \frac{2V_I}{\pi}\sin\left(\frac{\pi D}{2}\right) = 114.64\ \text{V}. \tag{5.1}$$

The components of current I_m is expressed as

$$I_C = \frac{-V_e\alpha}{\alpha^2 + \beta^2} = \frac{-114.64 \times 97.1668}{97.1668^2 + 162.1639^2} = -0.3116\ \text{A}, \tag{5.1}$$

$$I_S = \frac{V_e\beta}{\alpha^2 + \beta^2} = \frac{-114.64 \times 162.1639}{97.1668^2 + 162.1639^2} = 0.54695\ \text{A}. \tag{5.1}$$

The components of current V_m is expressed as

$$V_C = \frac{-I_S}{C\omega_s} = \frac{0.54695}{2.17 \times 10^{-}9 \times 2 \times \pi \times 110 \times 10^3} = -348.6873\ \text{V} \tag{5.1}$$

$$V_S = \frac{I_C}{C\omega_s} = \frac{-0.3116}{2.17 \times 10^{-}9 \times 2 \times \pi \times 110 \times 10^3} = -207.73\ \text{V} \tag{5.1}$$

The magnitude of I_S and I_C is $I_P = \sqrt{I_C^2 + I_S^2} = 0.6294$ A.

With the evaluation of these parameters, the small-signal model can be derived. The transfer matrix is expressed as given in equation (4.108). Substituting the above parameters, we obtain,

$$\begin{bmatrix} \frac{d\hat{i_c}}{dt} \\ \frac{d\hat{i_s}}{dt} \\ \frac{d\hat{v_c}}{dt} \\ \frac{d\hat{v_s}}{dt} \\ \frac{dv\hat{_{Cf}}}{dt} \end{bmatrix} = \begin{bmatrix} -44.6 & -690 \times 10^3 & -892.06 & 0 & 562.59 \\ -690 \times 10^3 & -44.6 & 0 & -892.06 & -987.51 \\ 460 \times 10^6 & 0 & 0 & -690 \times 10^3 & 0 \\ 0 & 460 \times 10^6 & 690 \times 10^3 & 0 & 0 \\ -0.6432 & 0.3664 & 0 & 0 & -10 \times 10^3 \end{bmatrix} \begin{bmatrix} \hat{i_c} \\ \hat{i_s} \\ \hat{v_c} \\ \hat{v_s} \\ v\hat{_{Cf}} \end{bmatrix}$$

$$+ \begin{bmatrix} 0 & 0 & -0.54695 & 0 \\ 1.2732 & 0 & -0.3116 & 0 \\ 0 & 0 & 207.73 & 0 \\ 0 & 0 & 348.6873 & 0 \\ 0 & 0 & 0 & 460.8 \times 10^3 \end{bmatrix} \begin{bmatrix} \hat{v_i} \\ \hat{d} \\ \hat{\omega_s} \\ \hat{i_o} \end{bmatrix} \tag{5.0}$$

and the output matrix $\hat{v_o}$ is

$$[\hat{v_o}] = \begin{bmatrix} -0.0160 & 0.0091 & 0 & 0 & 0.02499 \end{bmatrix} \begin{bmatrix} \hat{i_c} \\ \hat{i_s} \\ \hat{v_c} \\ \hat{v_s} \\ v\hat{_{Cf}} \end{bmatrix} + \begin{bmatrix} 0 & 0 & 0 & 0.996 \end{bmatrix} \begin{bmatrix} \hat{v_i} \\ \hat{d} \\ \hat{\omega_s} \\ \hat{i_o} \end{bmatrix}. \tag{5.0}$$

6 Conclusion

6.1 Summary

- The steady-state frequency-domain analysis of the series resonant converter has been performed and various parameters namely, input impedance Z, resonant current I_m and voltage V_m and the voltage transfer functions M_{Vr} and M_V have been derived.

- Brief introduction to the parallel and series-parallel resonant converters has been provided. Their operation, characteristics, and applications have been discussed.

- The concept of extended describing function has been introduced. Using the non-linear state equations derived using first principles, the series resonant converter is modeled. Initially, based on first harmonic approximation, the steady-state parameters are derived. By perturbation about the steady-state operating point, a large signal model is derived. Linearizing the large-signal model and applying the small-signality conditions, the small-signal model is extracted.

- A design example is provided in order to determine the component values and component stresses. The first harmonic approximated steady-state parameters are also evaluated. Finally, the small-signal transfer matrix is obtained representing the small-signal model of the series resonant converter.

6.2 MATLAB Results

For the component values and the calculated parameters from the design of series resonant converter provided in Chapter 5, the steady-state quantities are plotted on the frequency-domain and the converter behaviour is analysed. Figures 6.1 and 6.2 represents the variation of input impedance $|Z|$ and ψ_Z with respect to the variation in

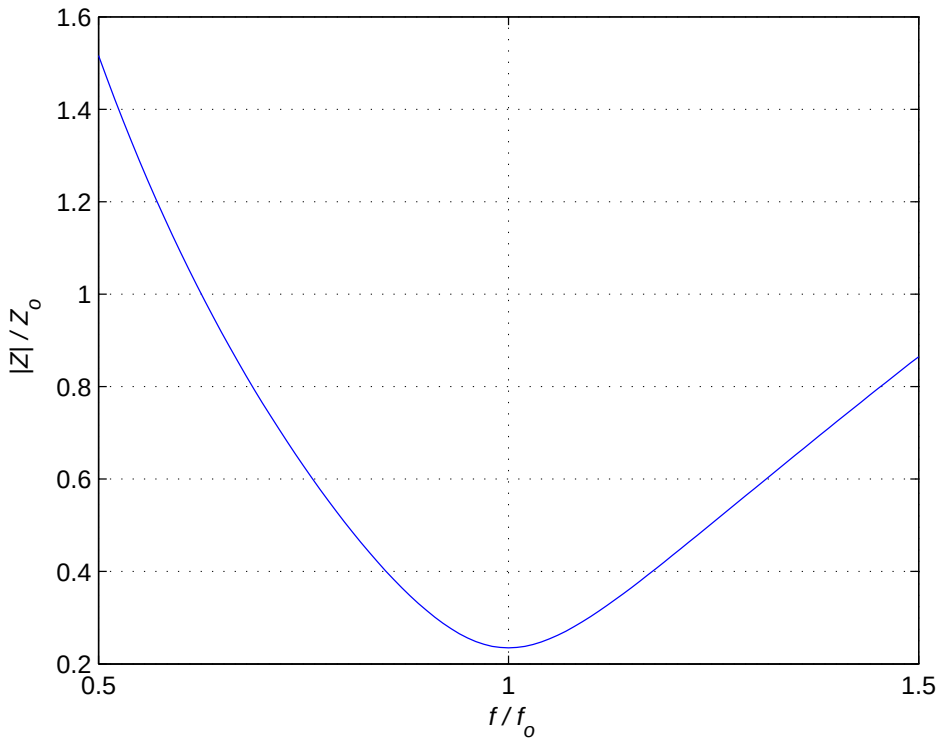

Figure 6.1: Magnitude of Z with variation in normalized switching frequency f/f_o

switching frequency. It is observed that for frequencies lower than f_o, i.e, for $f/f_o < 1$, ψ_Z is less than zero. This means that the resonant circuit offers a capacitive load to the flow of current and the current i_m leads the fundamental component of the voltage v_{s1}. When $f/f_o > 1$, ψ_Z is greater than zero. the resonant circuit offers inductive loading causing the current i_m to lag the fundamental component of v_s.

Figure 6.3 shows the plot of resonant circuit voltage gain M_{Vr} for different f/f_o. For the converter designed, it can be observed that, at $f/f_o = 1.07$, the resonant circuit voltage gain is approximately equal to the calculated value of 0.8664. Figure 6.4 represents the phase plot of the resonant circuit voltage gain. It can be observed that, the zero-crossing occurs at the resonant frequency. At this instant, the voltages across the inductor and capacitor are equal and opposite to one another and they cancel out. Due to this, the entire input voltage to the resonant circuit is completely

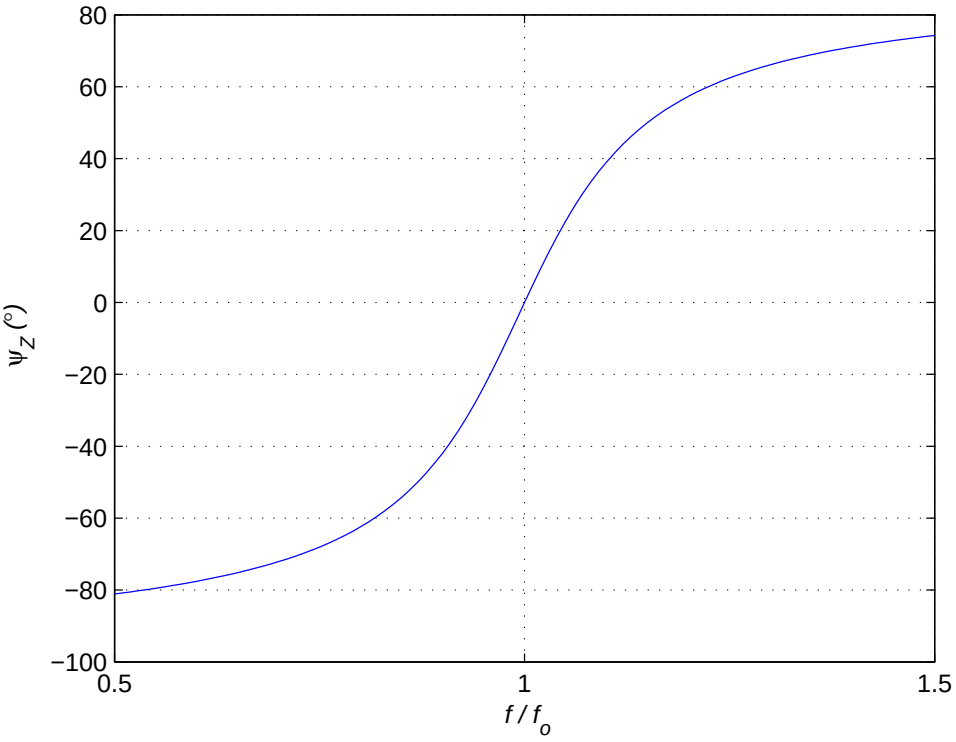

Figure 6.2: Phase of Z with variation in normalized switching frequency f/f_o

transferred to the rectifier. At frequencies below f_o, $\psi_{M_{Vr}}$ is greater than 0, indicating that, the current is being offered a capacitive load, causing a voltage to drop across it. Similarly, above f_o, $\psi_{M_{Vr}}$ is negative. The inductive reactance is greater, hence large voltage drop appears across the resonant inductance. Maximum power is transferred to the load when $f = f_o$. Figure 6.5 shows the total converter gain $M_V = V_O/V_I$. It is observed that with the bridge rectifier, M_V can not be greater than 0.5 at any operating frequency. This is advantageous since, the voltage stresses across the bridge rectifier diodes is moderated to a very low value as compared with the half-wave rectifier. Figure 6.6 shows the variation of steady-state voltage gain M_V with normalized switching frequency obtained using extended describing function. It can be observed that, the voltage gains plotted in Figures 6.5 and 6.6 are in accordance with one another. This validates the steady-state behaviour of the converter obtained

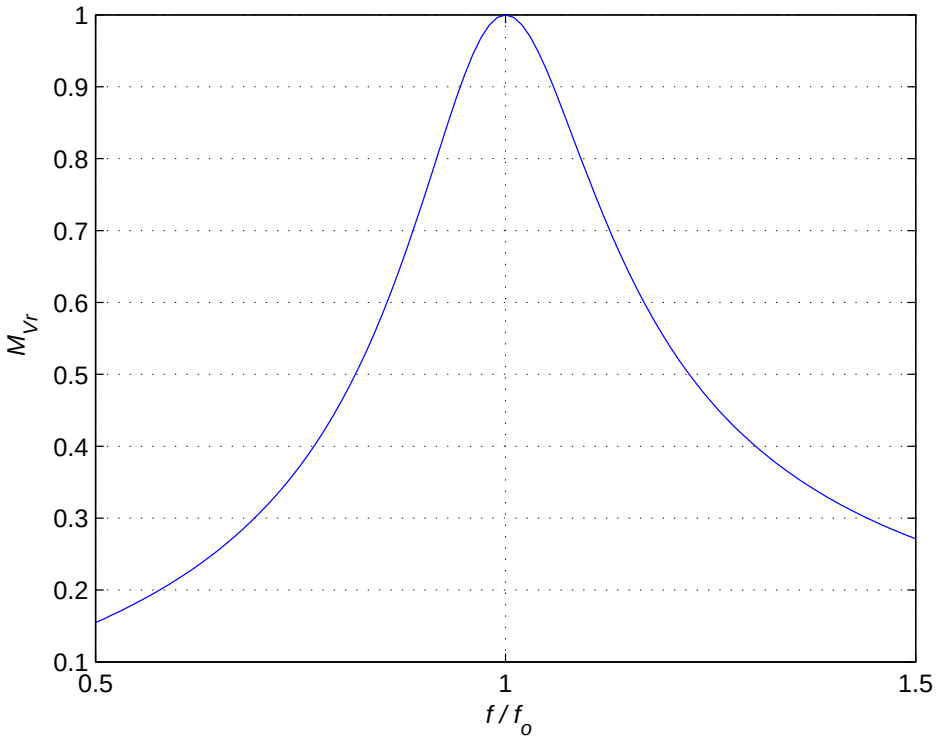

Figure 6.3: Magnitude of M_{Vr} with variation in normalized switching frequency f/f_o.

using first harmonic approximation.

Figure 6.7 represents the voltage stresses across L and C. At frequencies close to the resonant frequency, the stress across these components is maximum. Hence, operation at resonant frequencies is usually avoided and this is an important consideration especially when the load is short-circuited. Figure 6.8 shows the variation of total efficiency η of the SRC with load resistance R_L for the design provided. It is observed that, the efficiency increases with increase in the value of R_L. From Figure 6.8, the value of η at $R_L = 200\ \Omega$ is approximately 98 % and is in accordance with the designed values.

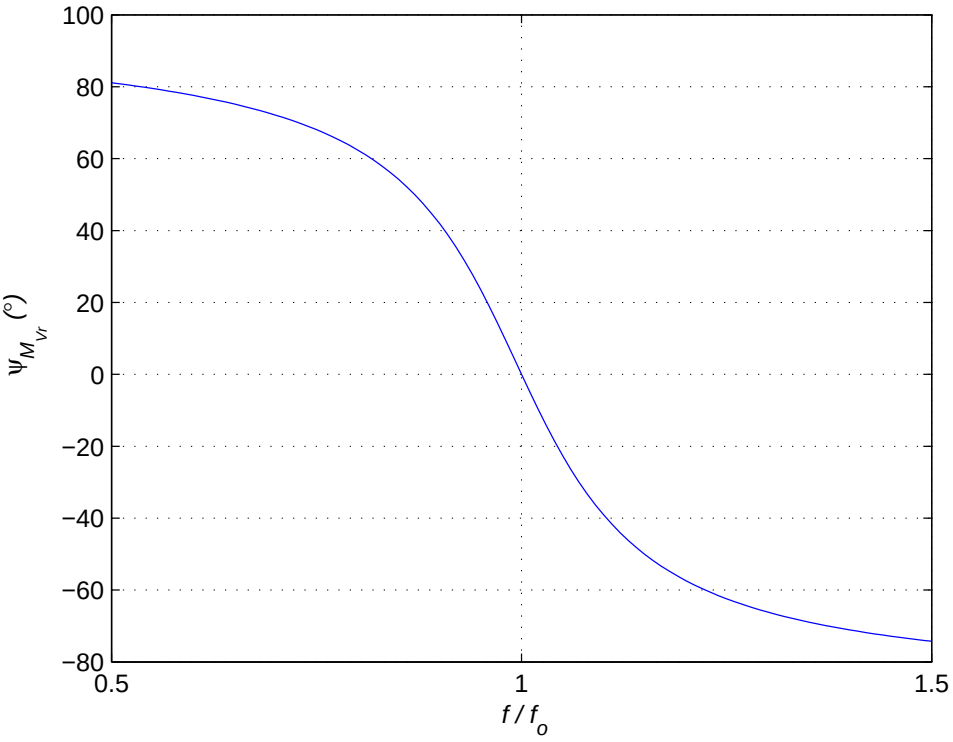

Figure 6.4: Phase of M_{Vr} with variation in normalized switching frequency f/f_o.

6.3 SABER Results

The design example provided in Chapter 5 is simulated on SABER circuit simulator. The components are chosen from the SABER MAST part library. The MOSFET chosen is MTP4N50 n-channel power MOSFET by FAIRCHILD SEMICONDUCTOR. The component specifications are provided in [24]. The inductor and capacitors are chosen from the MAST part library and their esr are assigned as considered in the design. The diodes used in the set-up of bridge rectifier is MUR10100 ultra-fast recovery diodes by MOTOROLA. The device specifications are provided in [25].

Figure 6.9 shows the schematic of the series resonant converter developed using SABER Sketch. The switches are provided with gate pulses at 110 kHz $\approx$ 9.09 ms and a delay of 4.54 ms between each turn-on. The calculated values of L and C are used. An ideal DC transformer with 1:1 turns ratio is used to cascade the resonant

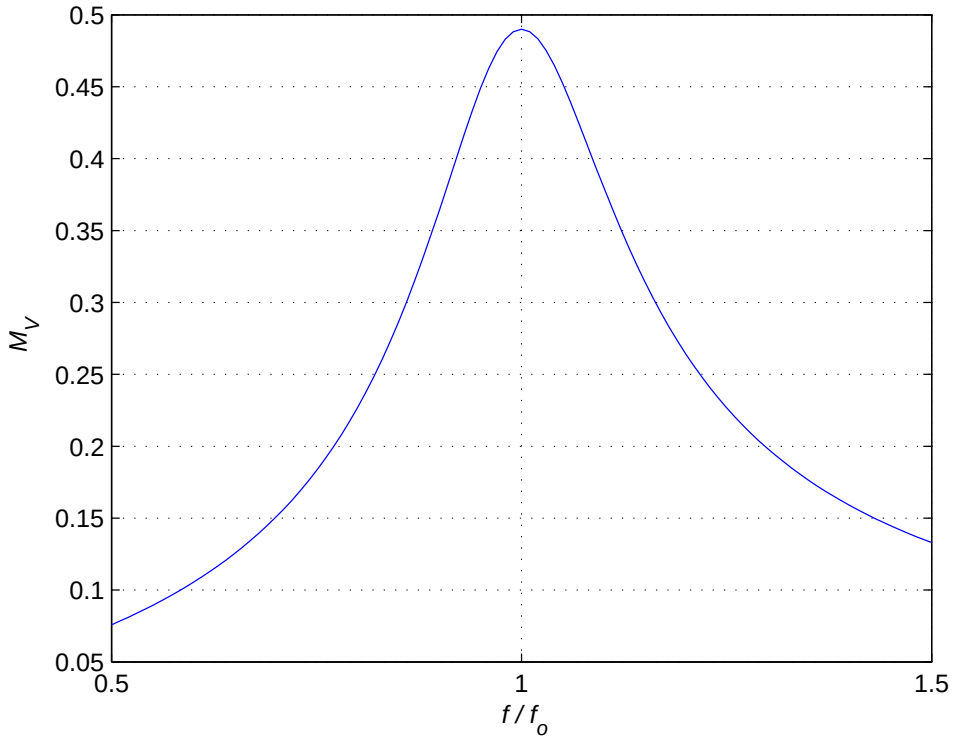

Figure 6.5: Magnitude of M_V with variation in normalized switching frequency f/f_o.

circuit with the bridge rectifier.

Figure 6.10 shows the voltage across the switches S_1 and S_2. The voltage $v_{DS2} = v_s$ is equal to the input voltage $V_I = 180$ V. Figure 6.11 shows the switch currents during their corresponding turn-on times. The maximum value of switch current I_{SM} is in accordance with the value obtained in equation (5.1.1). The negative current spikes flow into the source through the intrinsic anti-parallel diodes of the MOSFETs.

Figure 6.12 shows the voltage and current waveforms through the resonant capacitor and resonant inductor respectively with respect to the gate pulses. As calculated in the design, the maximum stress across the capacitor is found to be ≈ 488 V. From equation (2.5), it can be seen that $i_m = i_{S1} - i_{S2}$ and the peak current stress $I_{SM} \approx 0.58$ A as calculated.

Figures 6.13 represent the voltage across the individual diodes respectively. The

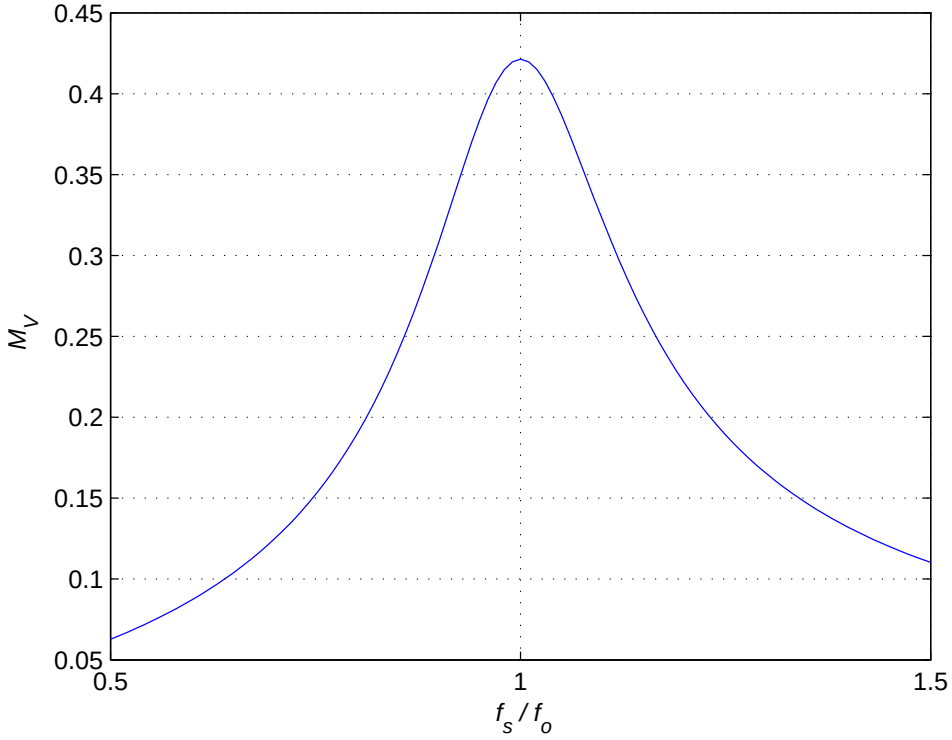

Figure 6.6: M_V as a function of normalized switching frequency f/f_o obtained using the extended describing function.

maximum stress across each diode in the bridge rectifier is equal $-V_O$. The current flowing through the diodes and rectified output current I_O flowing into the load is shown in Figure 6.14. The maximum value of output current is observed to be equal to 0.3771 A and is in accordance with the calculated value.

Figure 6.15 shows the transient response of the series resonant converter. For the designed values of components and frequency, the required output voltage of 75 V is achieved. For detailed analysis, Figure 6.16 depicts the average values of output current I_O, output voltage V_O and output power P_O. The average value of P_O is found to be equal to 28.132 W and is in accordance with the theoretically calculated values.

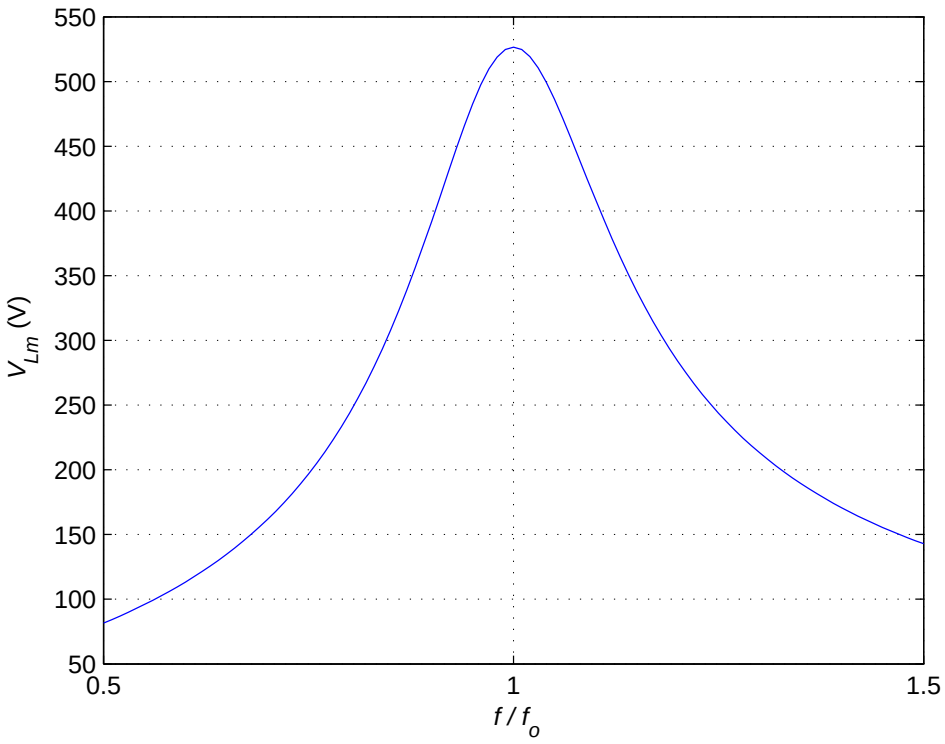

Figure 6.7: Variation of V_{Lm} with normalized switching frequency f/f_o.

6.4 Contribution

The resonant DC-DC converters are used in a myriad of applications which are powered either by the ac line supply or by batteries and fuel cells. Certain applications, for example, light emitting diode (LED) require drivers which should maintain constant current and constant voltage at their outputs. Any abrupt variations in the input signal will cause either an amplified or attenuated variation in the output voltage also. It is essential to understand the response of these converters towards such fluctuations so that proper control schemes can be used in order to regulate the output parameters with respect to a reference signal. Hence, a small-signal model is required. The extended describing function method to model a frequency controlled converter is well studied and applied to the series resonant DC-DC converters. The SRC considered is a half-bridge inverter at input end with a bridge rectifier at the

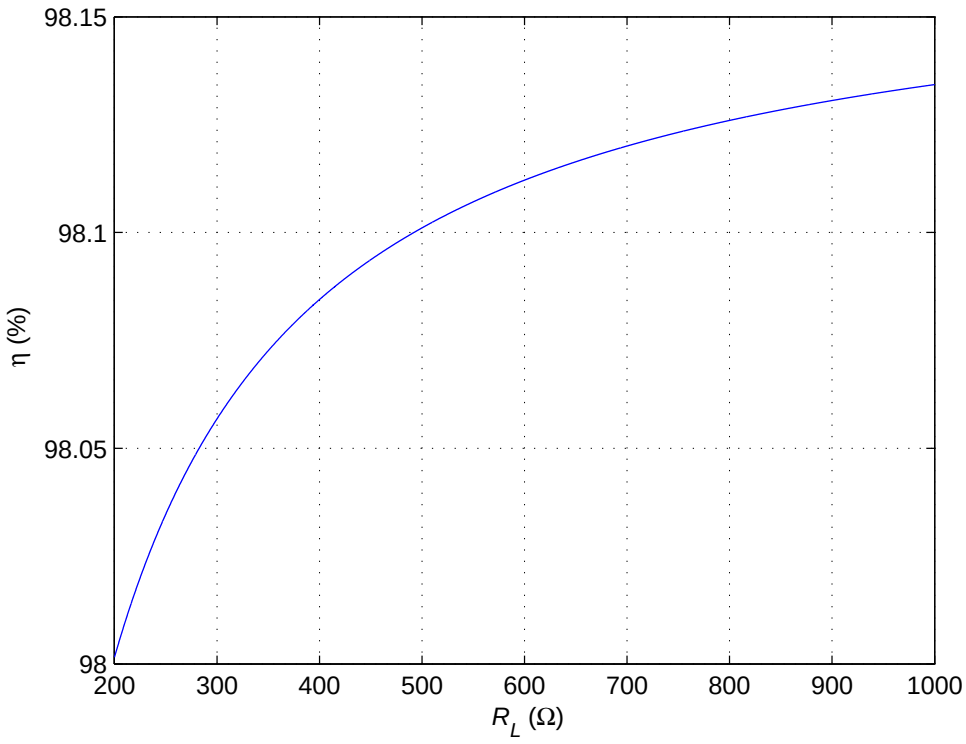

Figure 6.8: Variation of efficiency η with load resistance R_L.

output end. By performing first harmonic approximation of the state variables, a steady-state model is derived and then state-space averaging is performed to obtain a large signal model. Th steady-state voltage transfer function using first harmonic approximation is derived and plotted for the designed converter is and in accordance with that obtained using frequency-domain analysis. Furthermore, a transfer matrix has been derived which relates the small-signal state variables of the converter with the input and control parameters. The design example is simulated using SABER Sketch and is shown that the values obtained are in accordance with those calculated theoretically.

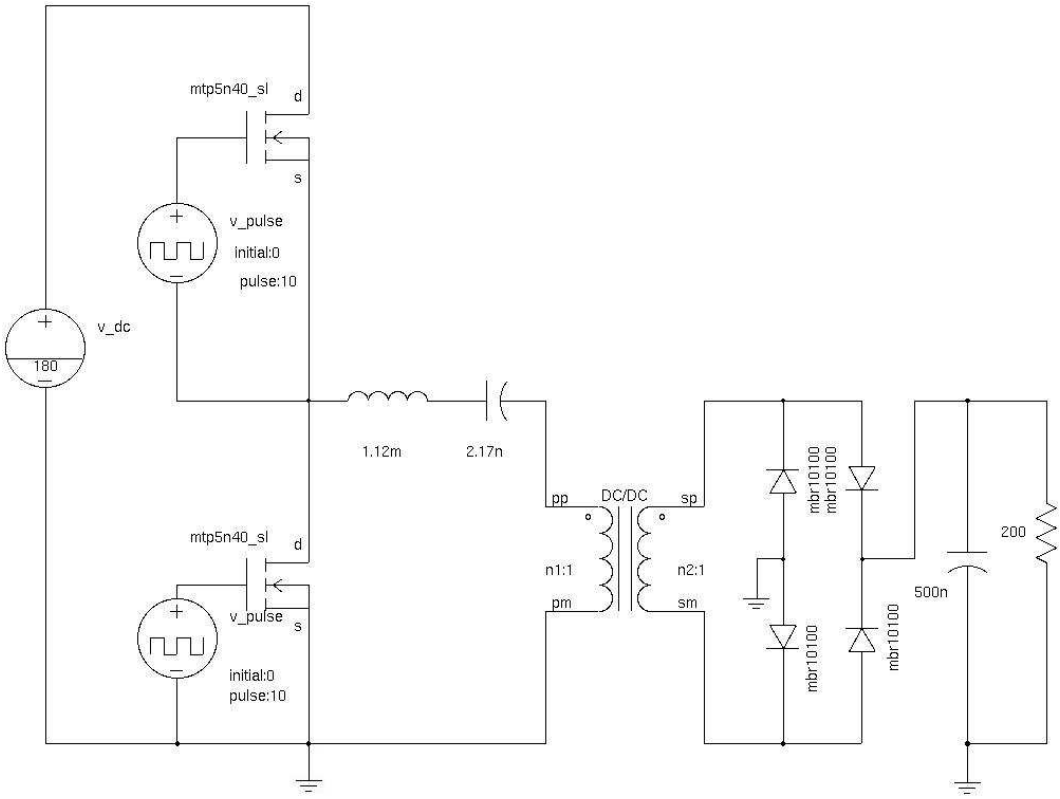

Figure 6.9: SABER schematic: Circuit of series resonant converter.

6.5 Future Work

Using the transfer matrix, in-depth analysis of various transfer functions can be performed. The applicability of this method on resonant converters with the inclusion of impedance-matching circuits for different types of loads (inductive and capacitive) can be studied. Since the analysis is based on energy storage elements, the applicability of this method on other forms of DC-DC converters can be tested.

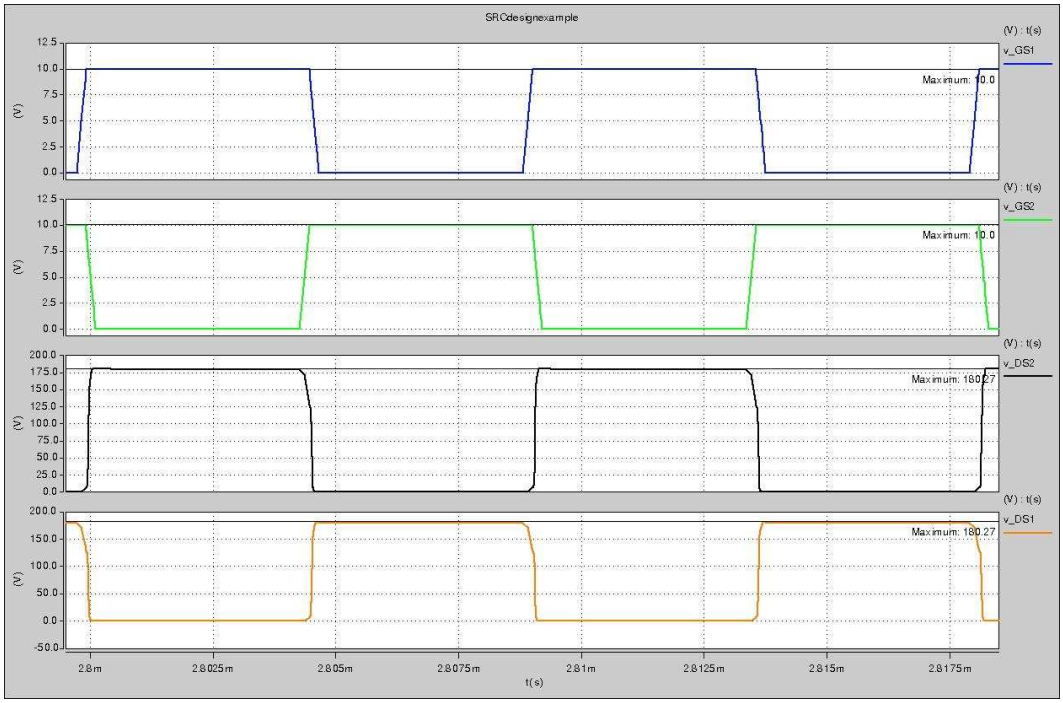

Figure 6.10: SABER plot: Switch voltages v_{DS1} and v_{DS2}.

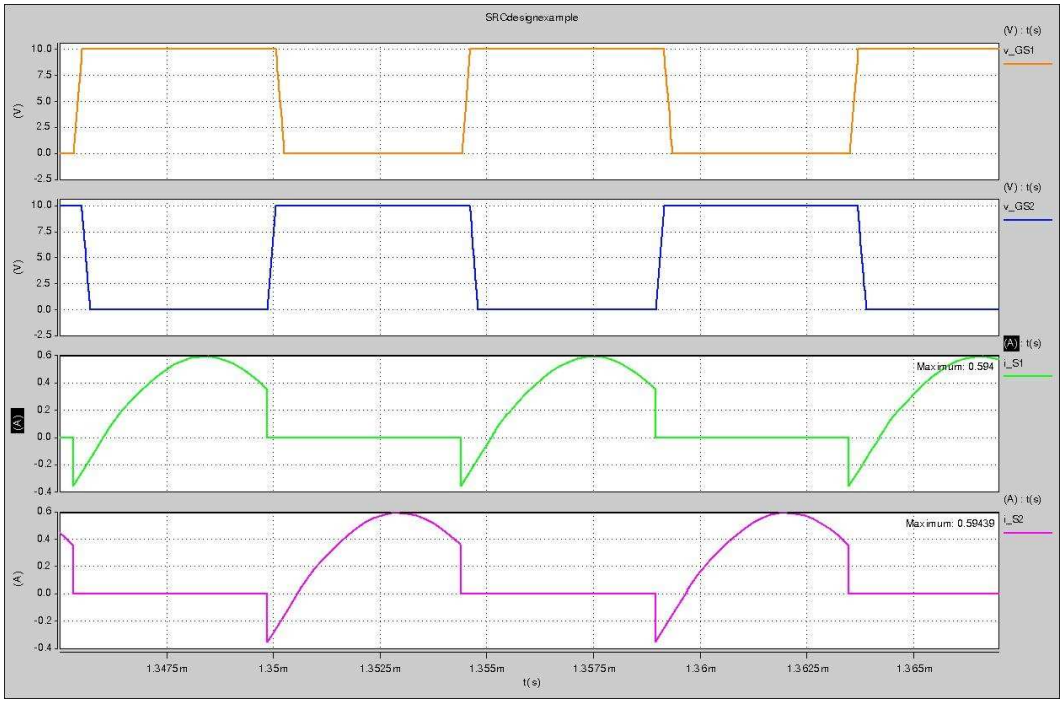

Figure 6.11: SABER plot: Switch currents i_{S1} and i_{S2}.

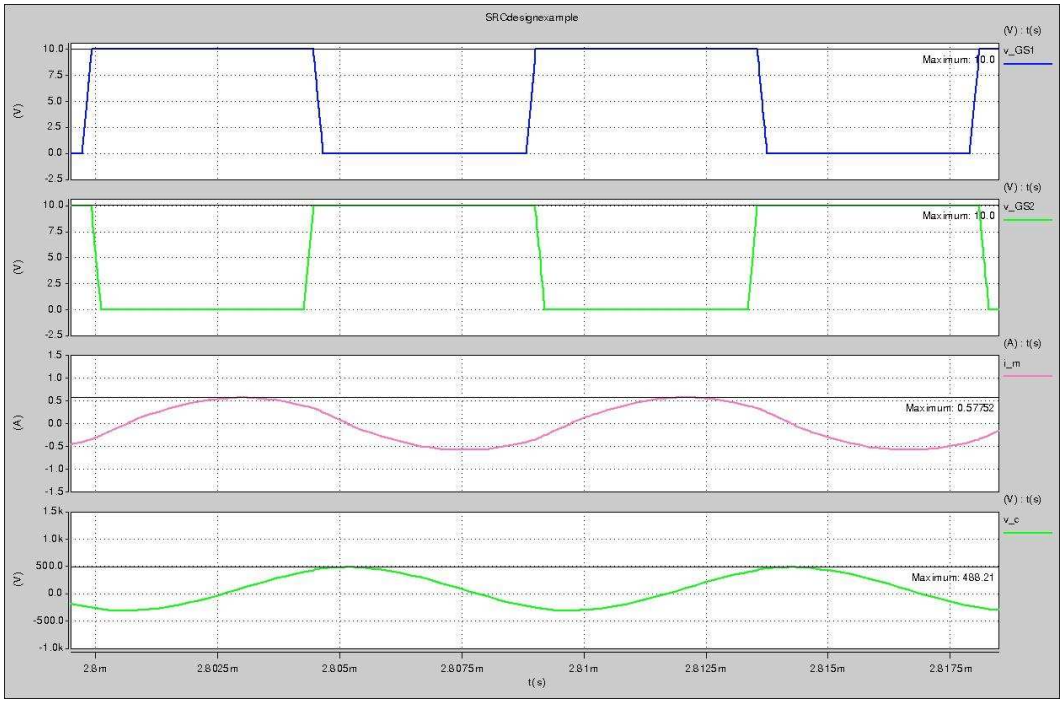

Figure 6.12: SABER plot: v_C and i_m during alternate switching cycles.

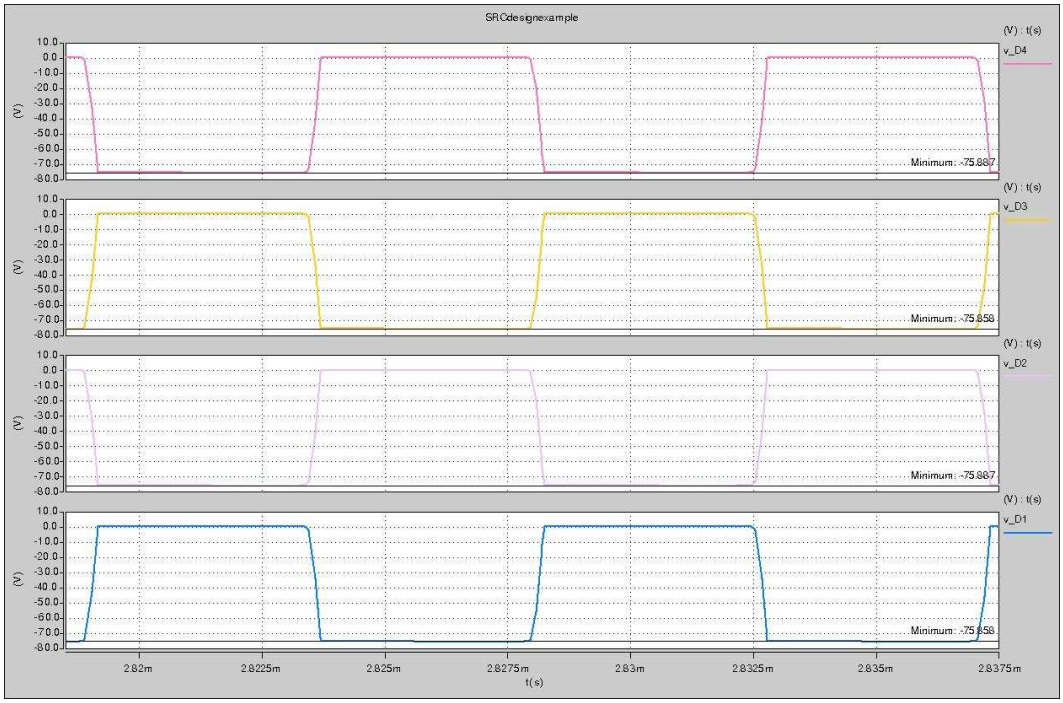

Figure 6.13: SABER plot: Voltages across D_1, D_2, D_3, D_4.

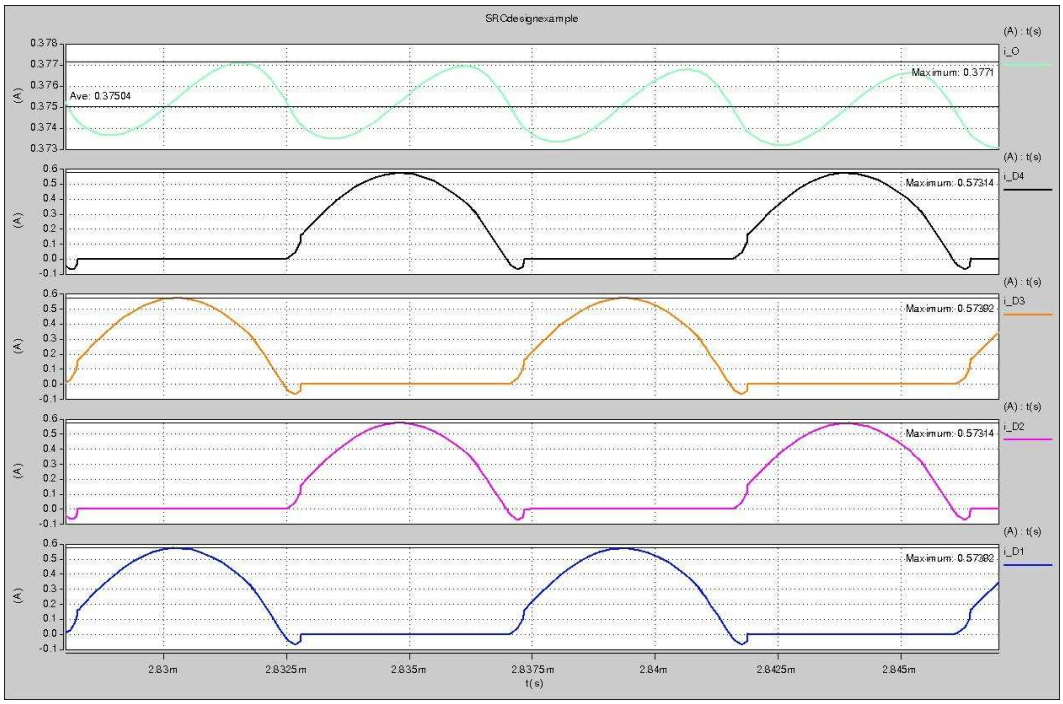

Figure 6.14: SABER plot: I_O and currents through D_1, D_2, D_3, D_4.

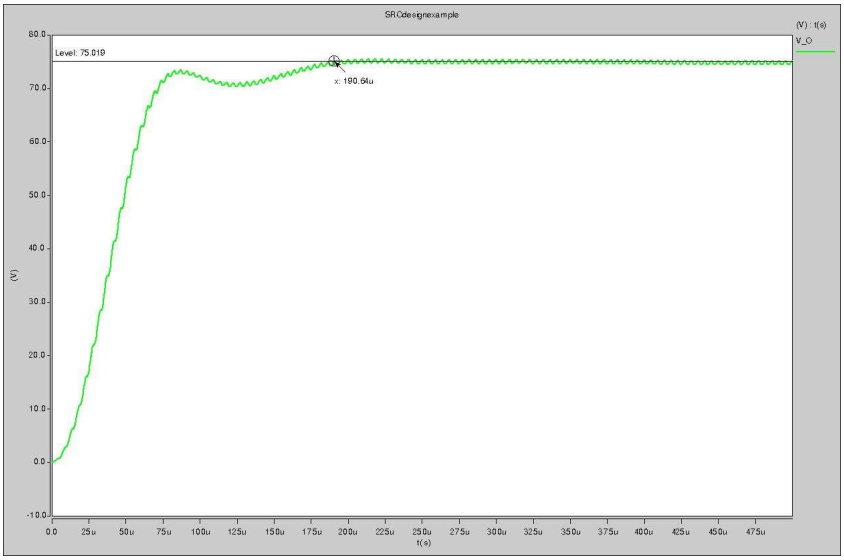

Figure 6.15: SABER plot: Transient response of V_O.

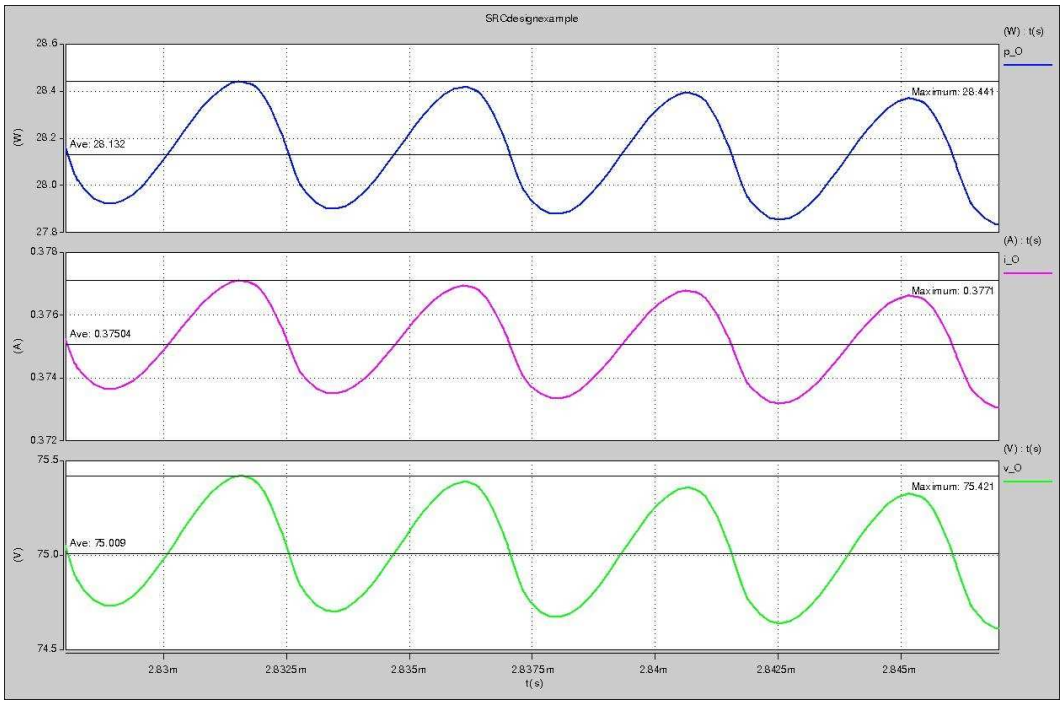

Figure 6.16: SABER plot: Average values of V_O, P_O, and I_O.

7 Bibliography

References

[1] M. K. Kazimierczuk and S. Wang, "Frequency-domain analysis of series resonant converter for continuous conduction mode," *IEEE Trans. Power Electron.*, vol. 7, no.2, pp. 651-659, April 1992.

[2] A. F. Witulski and R. W. Erickson, "Extension of state-space averaging to resonant switches and beyond," *IEEE Trans. Power Electron.*, vol. 5, no. 1, pp. 98-109, January 1990.

[3] A. F. Witulski, A. F. Hernandez, and R. W. Erickson, "Small-signal equivalent circuit modeling of resonant converters," *IEEE Trans. Power Electron.*, vol. 6, no. 1, pp. 11-27, January 1991.

[4] V. Vorperian, "Approximate small-signal analysis of the series and the parallel resonant converter," *IEEE Trans. Power Electron.*, vol. 4, no. 1 pp. 15-24, January. 1989.

[5] V. Vorperian and S. Ćuk, "Small-signal analysis of resonant converter," *IEEE Power Electronics Specialists Conf. Rec.*, pp. 715-705, 1985.

[6] V. Vorperian and S. Ćuk, "A complete DC analysis of the series resonant converter," *IEEE Power Electronics Specialists Conf. Rec*, Cambridge, MA, pp. 85-100, 1982.

[7] A. F. Witulski and R. W. Erickson, "Steady-state analysis of the series resonant converter," *IEEE Trans. Aerosp. Electron. Syst.*, vol. 21, no. 6, pp. 791-799, November 1985.

[8] G. W. Wester and R. D. Middlebrook, "Low frequency characterization of switched DC-DC converters," *IEEE Trans. Aerosp. Electron. Syst.*, vol. 9, no. 3, pp. 376-387, May 1973.

[9] S. Ćuk and R. D. Middlebrook , "A general unified approach to modeling switching dc-to-dc converters in discontinuous conduction mode," *IEEE Power Electronics Specialists Conf. Rec.*, Palo Alto, CA, pp. 36-57, 1977.

[10] R. D. Middlebrook and S. Ćuk, "A general unified approach to modeling switching-converter power stages," *IEEE Power Electronics Specialists Conf. Rec.*, Cleveland, OH, pp. 18-34, 1976.

[11] R. J. Dirkman, "Generalized state-space averaging," *IEEE Power Electronics Specialists Conf. Rec.*, pp. 283-294, 1983.

[12] A. R. Brown and R. D. Middlebrook, "Sampled-data modeling of switching regulators," *IEEE Power Electronics Specialists Conf. Rec.*, pp. 349-369, 1981.

[13] G. C. Verghese, M. E. Elbuluk, and J. G. Kassakian, "A general approach to sampled-data modeling of power electronic circuits," *IEEE Trans. Power Electron.*, vol. PE-1, no. 2, pp. 76-89, April 1986.

[14] F. C. Y. Lee, R. P. Iwens, Y. Yu, and J. E. Triner, "Generalized computer-aided discrete-time modeling and analysis of dc-dc converters," *IEEE Trans. Industr. Electron. Contr. Instrum.*, vol. IECI-26, pp. 58-69, May 1979.

[15] M. K. Kazimierczuk and D. Czarkowski, *Resonant Power Converters*, 2nd Edition, New York: John Wiley & Sons, Inc., 2011.

[16] M. K. Kazimierczuk, W. Szaraniec, and S. Wang, "Analysis and design of parallel resonant converter at high Q_L," *IEEE Trans. Aerosp. Electron. Syst.*, vol. 27, no. 1, pp. 35-50, January 1992.

[17] M. K. Kazimierczuk, N. Thirunarayan, and S. Wang, "Analysis and design of series-parallel resonant converter," *IEEE Trans. Aerosp. Electron. Syst.*, vol. 29, no. 1, pp. 88-99, January 1993.

[18] R. L. Steigerwald, "A comparison of half-bridge resonant converter topologies," *IEEE Trans. Power Electron.*, vol. 3, no. 2, pp. 174-182, January 1988.

[19] S. D. Johnson and R. W. Erickson, "Steady-state analysis and design of parallel resonant converter," *IEEE Trans. Power Electron.*, vol. 3, no. 1, pp. 93-104, January 1988.

[20] M. K. Kazimierczuk, *Pulse-width Modulated DC-DC Power Converters*, United Kingdom: John Wiley & Sons, Inc., 2008.

[21] B. P. Lathi, *Signal Processing and Linear Systems*, California: Berkeley-Cambridge Press, 1998.

[22] J. Martin-Ramos, J. Diaz, A. M. Pernia, M. J. Prieto, and F. F. Linera, "Modeling of the PRC-LCC resonant topology with a capacitor as output filter," *IEEE Applied Power Electronics Conf. Rec.*, vol. 2, pp. 1337-1342, 2002.

[23] E. X. Yang, F. C. Lee, and M. M Jovanovic, "Small-signal modeling of series and parallel resonant converters," *IEEE Applied Power Electronics Conference Conf. Rec.*, pp. 785-792, 1992.

[24] Fairchild Semiconductor, MTP4N50 n-channel power MOSFET datasheet, www.datasheetcatalog.com.

[25] Motorola, MUR10100 ultra-fast recovery diode datasheet, www.datasheetcatalog.com.